Research Repository UCD

Title	Vibration Resonance and Dynamic Characteristics of Pillared Phononic Crystals and Acoustic Metamaterials
Authors(s)	Gulzari, Muhammad, Lim, C. W.
Publication date	2023
Publication information	Gulzari, Muhammad, and C. W. Lim. "Vibration Resonance and Dynamic Characteristics of Pillared Phononic Crystals and Acoustic Metamaterials." Elsevier, 2023. https://doi.org/10.1016/b978-0-12-822944-6.00068-2.
Publisher	Elsevier
Item record/more information	http://hdl.handle.net/10197/26747
Publisher's version (DOI)	10.1016/b978-0-12-822944-6.00068-2

Downloaded 2026-05-01 23:51:35

The UCD community has made this article openly available. Please share how this access benefits you. Your story matters! (@ucd_oa)

© Some rights reserved. For more information

Vibration Resonance and Dynamic Characteristics of Pillared Phononic Crystals and Acoustic Metamaterials

Muhammad and CW Lim, Department of Architecture and Civil Engineering, City University of Hong Kong, Kowloon, Hong Kong SAR, P.R. China

© 2023 Elsevier Ltd All rights reserved.

Abstract

Engineered resonance phenomenon on surfaces have created an unprecedented world of surface science and technology. Branching resonant substructure as pillared phononic crystals and metamaterials emerge as a new class of synthetic structures with peculiar wave dispersion and dynamic properties that cannot be observed in natural materials. A fundamental property of interest includes dual behavior of pillared system that means exhibition of both Bragg and hybridization bandgaps. The rich resonance properties by this simple structure frontier a whole new research field in phononic crystals and metamaterials. The purpose of this article is to reproduce and combine different surface resonance phenomena reported in the literature on pillared structures with an insight on historical context, recent developments and future research prospects. The collection of findings reported here may provide a comprehensive insight on pillared resonances and help resolve the current challenges in the field to foster research spin-offs.

Key Points

- To provide an insight on phononic crystals and metamaterials, and to discuss their implications on breakthrough elastic waves control;
- To elaborate on enriched resonance properties of pillared phononic structures;
- To analyze dual behavior of pillared structures as phononic crystals and acoustic/elastic metamaterials;
- To investigate the surface resonance properties of pillared phononic structures for wave attenuation, waveguiding, sensing, focusing and defect analysis;
- To discuss the role of pillared resonances for local resonance and Bragg bandgaps enlargement;
- To explain the resonance properties of pillared system in the generation of topologically protected interface modes; and
- To summarize the recent developments in the field to foster research spin-offs.

 doi:10.1016/B978-0-12-822944-6.00068-2

Introduction

Vibration and noise are ubiquitous and they remain a fundamental problem in engineering sciences over a wide range of disciplines in basic research as well as practical applications, scaling from nano/micro mechanical/electromechanical systems to hazardous earthquakes, posing risks to lives and property of mankind. The advancement of present and future societies is dependent on sustainable, safe, efficient, and environmentally friendly technologies. Radically new approaches in civil infrastructure, transportation and energy production industries have substantially modified the urban and interurban vibrations and acoustic landscapes. Natural disasters, such as climate change and earthquakes, are other fundamental issues that require immediate and sustainable solutions. Vibration and noise mitigation are amongst other major challenges that need to be resolved. Breakthrough technologies and efficient approaches to cater these challenges are an essential and demanding field of research. Amongst various approaches developed during the last two decades, phononic crystals (PnCs) and acoustic metamaterials (AMs) have emerged as potential candidates for vibration and noise control due to their peculiar mechanical and dynamic characteristics, that are unattainable from naturally occurring materials. These fantastic wave phenomena are observed in the frequency bandgap (BG) region where wave propagation is restricted.

These functionally designed resonating structures have revolutionary capability to manipulate and shape the flow of photons and phonons with marvelous wave dispersion properties and dynamic characteristics that is inconceivable from natural designs and conventional materials. Although the history of periodic structures for waves manipulation is rather old, the history of *photonic crystals* is generally linked to the fundamental studies performed by Yablonovitch (1987) and John (1987). In such periodic system, the atoms are usually replaced with macroscopic media with varying dielectric constants and a periodic dielectric function is introduced to replace the periodic potential. The outcome yields novel engineered periodic system that exhibits photonic BG where the propagation of light and electromagnetic waves is prevented from propagating in a specific frequency range and a certain direction. Other unusual effective medium properties of interest revealed are negative refraction (Pendry, 2000), left-handed media (Koschny *et al.*, 2004), negative permittivity and negative permeability (Smith *et al.*, 2000), epsilon near zero media (Alu *et al.*, 2007) etc., with fantastic wave phenomena like rainbow trapping of light/ optical rainbow effect (Tsakmakidis *et al.*, 2007), hyperbolic metamaterials (Poddubny *et al.*, 2013), and techniques like transformation optics (Chen *et al.*, 2010) have been reported and applied for controlling the flow of light and electromagnetic waves. For more details one can refer to Muhammad *et al.* (2021a). Following these advancements, the field has seen a surge in research interest, as it has gradually taken on a multidisciplinary nature, covering both bulk and surface materials, as well as engineering features at the nanoscale, microscale, and macroscale.

The positive outcome in photonic crystals is further followed by phononic counterpart to control the acoustic and elastic waves that is referred as *phononic crystals*. The initial studies on PnCs with established wave dispersion characteristic is linked to the initial works by Kushwaha *et al.* (1994) and Sigalas and Economou (1994) . Later, Tanaka and Tamura (1998) developed numerical models to study the surface acoustic wave dispersion in two-dimensional (2D) periodic elastic structures. Likewise, multiple other studies have adopted the plane wave expansion method (Zhou *et al.*, 2018), wavelet based method (Yan and Wang, 2006), multiple-scattering theory (Kafesaki and Economou, 1999), boundary element method, finite element method (Muhammad *et al.*, 2021b) etc., to investigate the wave dispersion characteristics and peculiar dynamic properties of PnCs. These theoretical findings together with other investigations revealed effective medium properties like negative mass density (Huang *et al.*, 2009), negative moduli/ stiffness (Yu *et al.*, 2018), double negative medium (Prosandeev *et al.*, 2010), negative Poisson ratio, later referred as auxetic metamaterial (Ren *et al.*, 2018) etc., properties that are unobtainable in natural materials. Therefore, the discoveries in photonic crystals that is later followed by PnCs have now emerged as among the hot research topics with prominent engineering applications in future technologies. This new area, now known as *phononics* (Hussein and El-Kady, 2011), covers a broad variety of interconnected disciplines, including materials science, condensed matter physics, acoustics, electrical engineering, and mechanical engineering, to name a few.

A PnC, in more general terminology, is an artificial materials/structures made up of a periodic inhomogeneous elastic medium that can be used to control the movement of acoustic and elastic waves in solids, fluids or fluid-like solids. Floquet-Bloch theorem (simply expressed as $\mathfrak{F}(\mathbf{r}+\mathbf{R}) = e^{i\mathbf{k}.\mathbf{R}}\mathfrak{F}(\mathbf{r})$, where $\mathbf{R}$, $\mathbf{r}$ and $\mathbf{k}$ are the reciprocal lattice vector, position vector and wave vector, respectively) governs the propagation of acoustic/elastic waves in the PnC. The band structure/dispersion relationship over the *Brillouin zone* can be computed using this fundamental theorem (Muhammad *et al.*, 2019a). Before going into further details, some basic differences between the wave types in different media is necessary. In contrast to electromagnetic wave which are transversely polarized, the elastic waves in solid structures possess coupled longitudinal and transverse polarizations that make the design of structures with required BG even more cumbersome. Likewise, fluids only support longitudinal waves while solid materials contain both longitudinal and shear waves. Since wave polarization in solid structures is quite complex, therefore the challenge for designing of PnCs and AMs is both demanding and interesting in term of wave phenomena (Muhammad and Lim, 2020a; Muhammad *et al.*, 2019b; Chaplain *et al.*, 2020).

Further, here one may get confused between PnCs and AMs. The fundamental limitations in PnCs resulted in the discovery of novel resonating type of synthetic structures that is termed as AMs since pioneering work of Liu *et al* (2000). Before going into further details, it is necessary to mention that the abovementioned effective medium properties are related to AMs and it should not be confused with PnC counterpart. Also, a clarification on the difference between PnCs and AMs is equally important. Generally, these two terms are used in the literature interchangeably. Although both terms belong to artificial structures, governing frequency BG property, several differences are apparent. Briefly, PnC is a periodic structure with elasticity modulus/density contrast that works on the principle of Bragg effect, which means that the BG is generated due to structure's periodicity effect and destructive interference phenomena. Therefore, the opening of BG frequency is dependent on the periodicity constant (wavelength). Adversely, AMs, which is occasionally referred to as elastic metamaterials or mechanical metamaterials, is a synthetic composite structure composed of inclusions/resonators that couple with hosting media to generate BG. The BG is solely generated

due to the coupling of local resonance of the resonators/inclusions with waves propagating in the host media. Usually, the BG is induced at much lower frequencies (subwavelength scale), compared to the Bragg mechanism. In addition, these artificial composite structures can be periodic or aperiodic and due to the local resonance mechanism, the system's periodicity possesses limited effect on the opening and closing bounding edges of the BG. In fact, the opening of BG at subwavelength scale provides promising avenue to manipulate waves of very low frequency (large wavelengths) with much smaller unit cell structure. In literature the term subwavelength resonator is referred to highlight this characteristic. Due to this property, AM is considered as a homogeneous material/continuum structure with effective medium characteristics, which can be negative under specific conditions. A detailed explanation on the negative effective medium properties and PnCs and AMs historical context is given in Muhammad *et al.* (2021a). Due to the Bragg effect and system's periodicity, the PnC is not recommended for low frequency wave manipulation as large size periodic structures are required. Conversely, AM is considered as a prominent candidate for low frequency wave manipulation due to subwavelength resonator size, effective medium properties, and local resonance mechanism.

This book article's main goal is to present the properties and functionalities of a particular form of phononic structure suggested over a decade ago and consists of array of pillars on a plate substrate. Due to the structural configuration, this so-called pillared PnC/AM is characterized as 2-D material system that means, it has a Brillouin zone that is definable in two-dimensional space and the branching pillars work as local resonators. Thus, identical to bulk AM proposed by Liu *et al* (2000), the phenomenon of local resonance/wave hybridization prevails in 2-D medium or surface. In addition, Bragg BG is also evident due to periodic arrangement of the pillars and structural morphology. Therefore, this dual aspect allows this class of material system to act as both a PnC and an AM. Besides, when the pillars are arranged at the surface of semi-infinite half space, the outcome resulted in an elastic metasurface with unusual wave phenomena and dynamical characteristics (Su *et al.*, 2018; Zeighami *et al.*, 2019; Muhammad *et al.*, 2020). For instance, when the pillars are arranged over a half-space, subwavelength waveguiding and multiplexing phenomena is evident (Muhammad *et al.*, 2020). Likewise, by manipulating the geometric parameters of the pillars, subwavelength wave dispersion properties can be altered over a desire frequency range.

Pillared Phononic Crystal and Metamaterial

Recent Developments

This section gives a literature survey on pillared structures working as PnC and AM. The initial studies on pillared metamaterial is related to the first studies conducted by Pennec *et al.* (2008) and Wu *et al.* (2008) where single pillar supported on periodic plates is considered. This fact is substantiated that, if geometric parameters of pillar-plate structure are selected wisely, low-frequency subwavelength BG below Bragg BG resulting from local resonance mechanism can be obtained. This subwavelength BG is induced due to the avoided crossing between a pillar resonant mode and a wave dispersion branch of the plate mode. Following the initial works, subsequently low-frequency BG in the wide frequency spectrum is experimentally validated (Wu *et al.*, 2008; Achaoui *et al.*, 2011; Rupin *et al.*, 2014). Since the width and position of BG is dependent on both pillar and plate resonant modes coupling, there exist a range of possibilities for modifying the geometric parameters and/or material composition to tune the BG properties. Some studies reported that designing the connection between pillar-plate structure, such as those consist of conic angle (Zhang *et al.*, 2012), relatively narrow neck (Bilal and Hussein, 2013; Li *et al.*, 2017), soft material like rubber (Oudich *et al.*, 2010; Li *et al.*, 2015; Muhammad and Lim, 2020b) do allow shifting of BG to a low-frequency region. This geometrical variation is analogous to reducing the "stiffness" in a mass-spring chain that is used as an idealized model to study the local resonance mechanism (Huang *et al.*, 2009; Hussein *et al.*, 2014; DePauw *et al.*, 2018). Further, the shape and resonant pillars symmetry type are other dominant parameters that are found impactful on the local resonance BG, especially on the width and position of BG (Khelif *et al.*, 2012). The embedment of pillars on both side of the plate provides another additional platform to enrich the design space. Provided that the geometric parameters of pillar such as height and diameter remain the same on both sides of plate, the coupling of identical resonant modes amplify the width of local resonance BG (Muhammad and Lim, 2020b). As stipulated above, local resonance BG is not dependent on system periodicity, thus the localized modes of pillar and plate structure can be further manipulated via introducing hollow parts in the pillars (Jin *et al.*, 2016a; Muhammad *et al.*, 2020). Likewise, filling those hollow parts with liquid results in the generation of solid-liquid coupling modes that can be further controlled/tuned by managing the filling height (Jin *et al.*, 2016b; Wang *et al.*, 2017; Zaremanesh *et al.*, 2021).

Apart from altering the geometric parameters of pillars, the low-frequency local resonance BG can also be controlled by removing some portion of the plate area or replacing those parts with some soft materials. In this aspect, *trampoline metamaterial* (Bilal and Hussein, 2013; Muhammad and Lim, 2020b; Bilal *et al.*, 2017) encompassing trampoline effect caused by periodic drilling of holes inside the plate caught enormous research interest. The effectiveness of such approach is validated both numerically and experimentally (Bilal *et al.*, 2017; Muhammad and Lim, 2020b). It is substantiated that removing a certain plate area confining the pillar reduces the plate stiffness and results in the springboard effect. Since a lesser area of the plate confines the pillar, an intensive vibration or, in other words, wave mode coupling of pillar and plate results in low-frequency and wider BG (Muhammad and Lim, 2020b). Further, an increase in plate hole diameter enhances the wave mode coupling and this is proven as another effective approach to enlarge the width of local resonance BG.

Moreover, the properties of BG can be actively controlled by piezoelectric shunted transducer (Zou *et al.*, 2016) or using magnetostatic field (Zhou *et al.*, 2016) or electromechanical coupling effects. Similar to pillar on a plate supporting symmetric (S_0) and anti-symmetric (A_0) Lamb modes, the arrangement of pillars on a semi-infinite substrate was also studied theoretically and

experimentally with a more emphasis on their local resonance BGs. The coupling of *photonics* and *phononics* has given rise to a new wave of applications known as the so-called *phoXonic materials* (Rolland *et al.*, 2012). For instance, pillared metamaterials can be designed that can exhibit both photonic and phononic BGs for simultaneous localization and tailoring of light and sound waves (El Hassouani *et al.*, 2010; Djafari Rouhani *et al.*, 2011). The term PhoXonic crystal is introduced and research work is being performed actively for designing metamaterials to be deployed for simultaneous photonic and phononic applications.

When AM is characterized, generally monopole and dipole resonant modes are related to negative effective compressibility and negative effective mass density, respectively, when examined within the scope of local resonance BG. However due to the lack of precise effective medium theory, the analysis of negative effective mass density or compressibility is rather more difficult as compared to the conventional 1-D, 2-D or 3-D AM models. This is due to the complex vibration of pillar structure with its base plate. Nonetheless, a pillared metamaterial, on the other hand, can also be thought of as a homogenous plate with anisotropy in the effective wavenumber (Williams *et al.*, 2015) or mass density matrix (Oudich *et al.*, 2014) and negativity property in effective modulus (Williams *et al.*, 2015), density (Oudich *et al.*, 2014; Assouar *et al.*, 2016) or stiffness (Yan and Wu, 2017). Besides, the monopole and dipole resonant modes can be tuned through a proper choice of pillar geometric parameters to easily probe the condition for switching the effective medium negativity. Another problem of interest is the influence of pillar resonance on the scattering and transmission of a single or array of pillars that is subjected to an incident surface wave. In such cases, a phase shift between incident wave and radiated wave from pillar through wave transmission curve is observed. A good example is the Fano resonance that may be induced by incorporating two unidentical pillars in one unit cell along a single row of pillars (Jin *et al.*, 2017). Likewise multilayer materials in the form of 1-D PnC also allow the localization of in-plane wave (Muhammad *et al.*, 2021b) and surface Rayleigh wave (Oudich *et al.*, 2017, 2018). In such geometrical configuration, the interaction of incident wave with resonant modes of the multilayer ridge structure resulted in a sharp transmission peak captured from the wave transmission curve. Corresponding to the transmission peak frequency, wave energy is robustly confined in the defected structure. Beside these developments, metasurfaces that are actually very thin structures arranged at the subwavelength scale have the capability to manipulate sound (or light) wave and disseminate interesting wave phenomena like anomalous reflection, refraction, focusing, high transmission with 2π phase shift or imaging phenomena. Line of pillar structures embedded at the plate surface and/or a substrate can also provide new tools for exhibiting identical features by manipulating Lamb waves in plate and surface Rayleigh wave or Love wave for deep substrates.

Potential Applications

In an application point of view, the pillared phononic crystals and metamaterials can be divided into a number of categories. However, in this article the following six categories are formulated with a brief discussion. (1) *Anomalous refraction and lensing properties*. An appropriate choice of pillar in periodic host media can reveal negative refraction effect provided that the group and phase velocities of dispersion branch reveal opposite sign leading towards negative effective refractive index (Djafari-Rouhani *et al.*, 2010; Addouche *et al.*, 2014; Yan *et al.*, 2013). This is also possible if the group velocity and phase velocity have an identical sign while the convexity of the iso-frequency contour demonstrate negative refraction (Al-Lethawe *et al.*, 2012). The later mechanism leads to high-resolution subwavelength superlensing effects (Rupin *et al.*, 2015). (2) *Wave attenuation*. As elaborated above, structural configuration of the pillared structure facilitates generation of both Bragg and subwavelength local resonance BGs. Such characteristics enable prominent applications in vibration attenuation facilities in sonic (Oudich *et al.*, 2010; Oudich *et al.*, 2011; Assouar *et al.*, 2016) and elastic (Wu *et al.*, 2008; Rupin *et al.*, 2014; Muhammad and Lim, 2020b; Muhammad *et al.*, 2020,2021b) frequency regimes. An ultrawide BG can also be obtained either by coupling the local resonance and Bragg BG (Badreddine Assouar *et al.*, 2014; Jin *et al.*, 2016c) or introducing composite structural configuration with trampoline effect (Bilal and Hussein, 2013). By enlarging the pillar structure in macroscale, the seismic Rayleigh wave can be attenuated or even the wave flow can be shaped to ensure protection of civil infrastructures (Colquitt *et al.*, 2017; Muhammad *et al.*, 2021c; Muhammad and Lim, 2021b). Energy harvesting/harvester devices are other prominent applications where the localize modes of the pillar is confined inside the BGs and electromechanical coupling effect can be manipulated (Carrara *et al.*, 2013; De Ponti *et al.*, 2020). (3) *Defect state, waveguiding, sensing and filtering*. The BG property also enables the propagation of localized energy in different paths if the traveling frequencies is managed within the Bragg and/or local resonance BGs. This is possible by designing waveguide on the host periodic medium as recently proposed by Jin *et al.* (2016a) for Lamb waves and Muhammad *et al.* (2020) for SAW. Such strategic design intervention helps induce localized/confined wave modes inside the BGs, thus allowing desirable wave propagation in certain designated paths. (4) *Gradient resonant phononic devices*. A focusing point can be achieved beyond the diffraction limit by employing a resonant pillar and a gradient index lens (Zhao *et al.*, 2016). By gradual variation of pillar height, resonant metalenses for flexural wave manipulation is designed (Colombi, 2016). Likewise, the metawedge phenomena (Colombi *et al.*, 2016a), Umklapp effect (Chaplain *et al.*, 2020) and wave mode conversion for Rayleigh wave to bulk shear and compressional waves are also proposed (Colombi *et al.*, 2016b; Muhammad *et al.*, 2021c). In another work, Guo *et al.* (2017) investigated the guiding of elastic waves through graded radius of pillars embedded on the host plate structure. (5) *Pillared metasurfaces*. Metasurfaces are generally refereed as tiny structures placed on the surface of host media with subwavelength thickness. Such setup can steer incoming waves in amazing ways by manipulating abrupt phase profile at the surface (Tang *et al.*, 2014; Assouar *et al.*, 2018). The interesting properties include anomalous focusing and imaging, reflection and refraction phenomena. This is a promising avenue especially when manipulation of Lamb waves on the plate and SAW on semi-infinite half-space is required. (6) *Phononic pillar graphene*. The hexagonal arrangement of pillars on the plate can be conceived as spring loaded resonators with peculiar dynamic properties analogous to graphene in elastic media (Torrent *et al.*, 2013).

Such arrangements also reveal topological properties in the form of zig-zag edge state, protected interface modes and edges modes (Miniaci *et al.*, 2018; Zhou *et al.*, 2020) etc. The *hypersonic phononic metamaterial* is another avenue where pillar-plate configuration has been investigated and the presence of BG is envisaged by Brillouin light scattering spectroscopy (Graczykowski *et al.*, 2012; Trzaskowska *et al.*, 2013). Nanophononic metamaterial (Davis and Hussein, 2014; Hussein *et al.*, 2020) is another concept proposed by Hussein *et al.* (2020) to reduce the phononic lattice thermal conductivity at nanoscale. Likewise multiple other works have studied pillar resonance to not only control the thermal conductivity but also thermoelectric conversion mechanism.

The major purpose of this article includes a literature overview on pillared phononic crystal and metamaterial and to study the resonant properties for waveguiding and localization, defect analysis and vibration attenuation purposes. The article is divided into eight sections. The abovementioned parts have provided a background and overview with historical context and state of the art research in the field of PnCs and AMs in general while pillared structures in phononic system in particular. The potential application of pillared materials and structures is also discussed. For a basic theoretical model one can refer to Yabin *et al.* (2021). Section "Wave Propagation in Pillared Phononic Systems" discusses the resonance properties of a fundamental pillared phononic crystal and metamaterial with BG opening subjected to Lamb waves and surface acoustic waves. In Section "Whispering Gallery Modes of the Hollow Phononic Pillars", the whispering gallery modes of hollow phononic pillars subjected to Lamb waves and SAWs are studied. The subwavelength waveguiding and wave multiplexing effects by an array of hollow and solid phononic pillars are demonstrated. Section "Resonances in Multilayer Phononic Pillars" puts forward an insight on the multilayer phononic pillars and their resonance properties for Lamb waves and SAWs attenuation and localization are investigated. An overview on pillared acoustic metamaterials to enlarge the Bragg and local resonance BGs is covered in Section "Low Frequency Bandgap Engineering" where the idea of trampoline metamaterials, tailorable metamaterials and disorder rainbow metamaterial is discussed. The idea of topologically protected interface state and edge modes in the context of pillared PnC and AM is covered in Section "Topological Protected Phononic Pillared Structures". A general introduction is given that is followed by a brief discussion on topological edge states. Finally, a conclusion with an outlook on the future research spin-offs to foster research on pillared phononic system at various length scales with prominent applications is given in Section "Conclusion and Future Outlook".

Wave Propagation in Pillared Phononic Systems

A Basic Analytical Model

Basic analytical models based on 1-D monoatomic chain always remain as a potential source to explain the concept of PnCs and pillared structures. In this section, we will explain the phenomena of bandgap opening and defect states in simple mass-spring lattice that can be replicated to pillared structures. For instance, we consider a linear monoatomic chain with atomic mass m, which is connected with neighboring atoms with a force α and with lattice spacing between atoms a, see **Fig. 1**(a). The equation of motion in such system for the nth atom can be expressed as $\frac{m\partial^2 u_n}{\partial t^2} = \alpha(u_{n+1} + u_{n-1} - 2u_n)$ where $u_n(t)$ is the atomic mass displacement at time t. The propagating wave solution can be written as $u_n(t) = Ae^{i(kna-\omega t)}$ and the wave dispersion relation can be obtained as $m\omega^2 = 2\alpha(1 - \cos(ka))$ where ω and k are wave frequency and wavenumber, respectively, that result in a dispersion plot accessible to figure-out the passband and BG frequency regions, see **Fig. 1**(b). For a monoatomic chain, the wavenumber takes

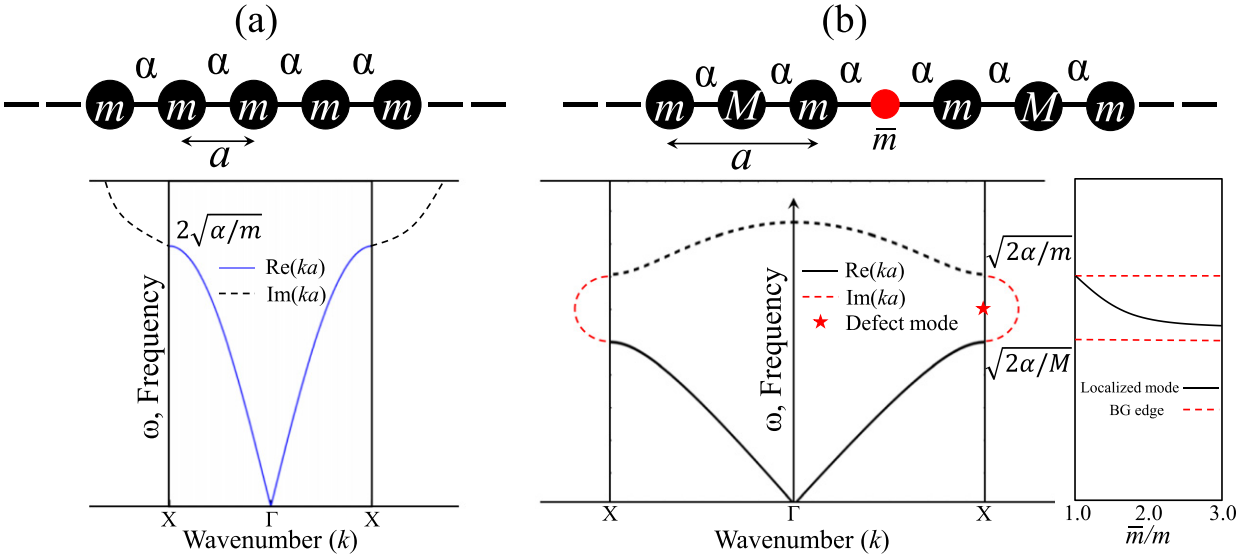

Fig. 1 (a) Monoatomic and (b) biatomic mass-spring model with the corresponding dispersion curves. The defect state in biatomic model is shown with a red dot. The localized mode caused by defect state is shown at the inset of dispersion plot enclosed by acoustic and optical branches. The variation of defect frequency with changing $\overline{m}$ is highlighted.

a positive value limited to $\omega_{max} = 2\omega_0$ where $\omega_0 = \sqrt{\alpha/m}$ is the system natural frequency (Hussein *et al.*, 2014; Muhammad and Lim, 2021c). Above ω_{max}, the wavenumber k becomes complex and wave cannot propagate in the system.

Now a defect mode in the form of a smaller mass $\overline{m} < m$ if introduced at the array location $n = 0$, the solution of equation of motion will give a localized mode at the frequency above $\omega_{max} = 2\omega_0$. If one analyzes the eigenfunction, a decaying energy field on both sides far from the defect state can be seen. Such an example is shown in **Fig. 1**(b). The effect is analogous to the presence of defect or cavity mode inside a hollow PnC. In contrast, when $\overline{m} > m$ the defect state cannot exhibit a localized mode rather it will disturb the local density of eigenstates in the frequency range below ω_{max}, that lie somewhere in the passbands.

The abovementioned analysis can be extended to biatomic linear mass-spring chain where two different masses m and M are connected with a force/spring constant α. By solving the wave dispersion relation of the biatomic linear chain, the band structure with BG bounded by the acoustic and optical branches can be observed. Now if a defect mass $\overline{m}$ is inserted inside this system at location $n = 0$, the defect frequency can be observed and adjusted by varying $\overline{m}/m$ inside the BG across a range of frequencies, see **Fig. 1**(b). Multiple other scenario can be considered by changing position or mass $\overline{m}$, another force α', changing the force α with nonlinear spring etc., and the wave dispersion characteristics with localized modes can be studied. Such investigations have already been covered in various studies (Hussein *et al.*, 2014; Banerjee *et al.*, 2018; Yabin *et al.*, 2021) and a detailed analysis is outside scope of this work.

Dual Nature of Pillared Phononic Crystal and Metamaterial

The study of absolute BG in PnCs has received enormous attention, especially for applications like waveguiding, confinement, filtering etc. This subsection will review the basic band structure properties of PnC plate which consist of a periodic arrangement pillars embedded on top of a thin homogenous elastic plate forming a square periodic array as shown in **Fig. 2**. The system periodicity that is dependent on Bragg BG and hybridization BG at low-frequency resulting from local resonance mechanism (pillars work as local resonators) can be observed simultaneously in such phononic system that articulate the dual aspects of pillared structure as PnCs and AMs. We illustrate this effect by considering steel pillars that are embedded on a silicon plate, as shown in **Fig. 2**. The mechanical properties are obtained from Pennec *et al.* (2008). By a wave dispersion study in 2D irreducible Brillouin zone, the eigenmodes in the form of reduced frequency $\omega a/2\pi v_t$ corresponding to a range of wavenumber is obtained as shown in **Fig. 3**.

The wave dispersion curve shown in **Fig. 3** corresponds to parameters with pillar height and radius $h/a = 0.6$, $r/a = 0.42$, respectively, and plate thickness $e/a = 0.1$. We observed three bands at low-frequency for X point in the Brillouin zone center that corresponds to the antisymmetric Lamb mode A_0, symmetric mode S_0 and shear-horizontal (SH_0) modes. With an increase in frequency, these three modes bend in a fashion that generate a narrow local resonance BG. This BG is situated at the subwavelength frequency regime where the lattice size is several orders smaller than the wavelengths being attenuated. In addition, within one frequency range, the pillar bending mode exhibits negative effective in-plane mass density while the associated compression resonant mode induces out-of-plane negative effective mass density within another frequency range. The overlap of these frequency regions results in the opening of subwavelength wave hybridization gap (Pennec *et al.*, 2008). The choice of geometric parameters is intricately tied to the simultaneous bending of acoustic branches and existence of this BG, as will be detailed later. Likewise, within the geometric parameters, a broad Bragg BG can also be seen due to the Bragg scattering effect as shown in **Fig. 3**.

A further and deeper insight on the vibration modes captured indicates that mode **Fig. 3**(i) and (iii) are associated with bending of pillars along with a stronger and weak bending motion of plate, respectively, as shown in **Fig. 3**. The resonant mode (ii) is completely a compression vibration mode of pillar along the z-direction (out-of-plane motion) corelated with a robust vertical deformation of the plate structure. Moreover, the opening of subwavelength hybridization BG is highly associated with vibration

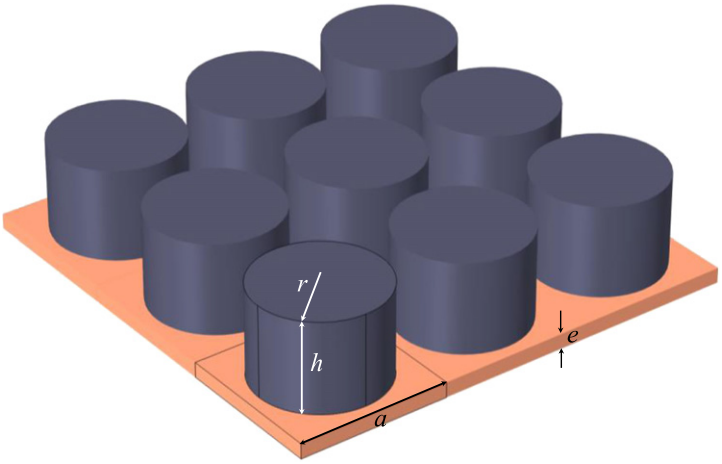

Fig. 2 Geometry of phononic pillar plate structure where the pillars are deposited on a homogenous plate. The periodicity constant is a and the pillar height and radius are h and r, respectively. The homogenous phononic plate thickness is e.

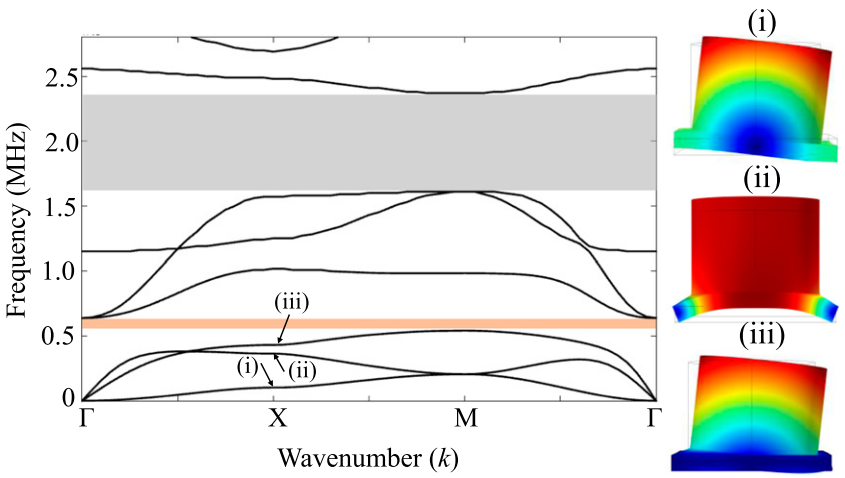

Fig. 3 Band structure for the pillar-plate phononic system with pillar height and radius as $h/a = 0.6$, $r/a = 0.42$ and plate thickness $e/a = 0.1$. The local resonance and Bragg BGs are highlighted and resonant modes of the phononic system that exhibit local resonance BG is also highlighted on the right. The figure is based on results reported in Pennec *et al.* Reproduced from Pennec, Y., Djafari-Rouhani, B., Larabi, H., et al., 2008. Low-frequency gaps in a phononic crystal constituted of cylindrical dots deposited on a thin homogeneous plate. Physical Review B 78 (10), 1–8.

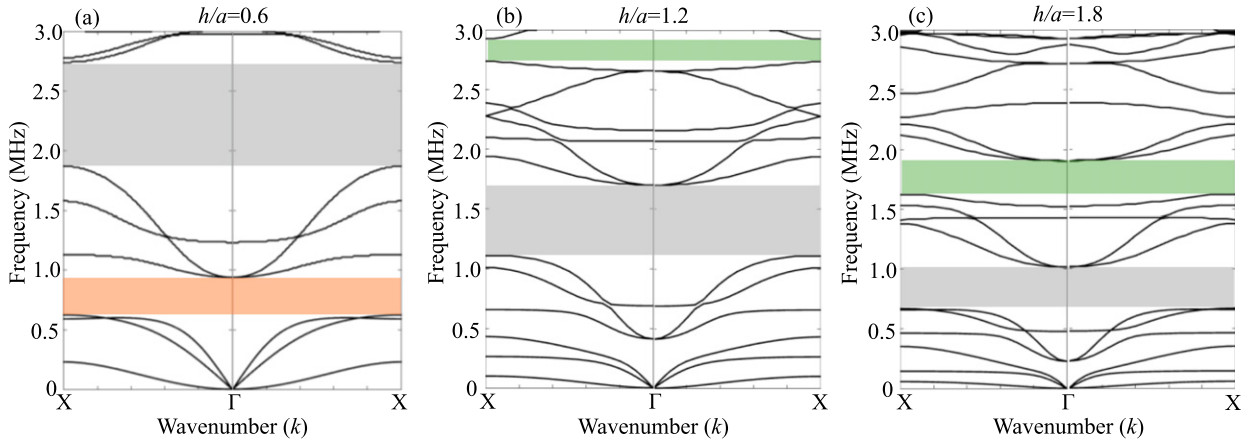

Fig. 4 Evolution of band structure with varying pillar height (a) $h/a = 0.6$ (b) $h/a = 1.2$ (c) $h/a = 1.8$. The geometric parameters include plate thickness $e/a = 0.2$ and pillar radius $r/a = 0.42$. The BGs are highlighted. The figure is based on results reported in Pennec *et al.* Reproduced from Pennec, Y., Djafari-Rouhani, B., Larabi, H., *et al.*, 2008. Low-frequency gaps in a phononic crystal constituted of cylindrical dots deposited on a thin homogeneous plate. Physical Review B 78 (10), 1–8.

modes (ii) and (iii). For further details about the effect of geometric parameters on the reported BGs, one can refer to Pennec *et al.* (2008). Here we only put forward a brief insight on the effects of varying pillar height on BGs.

In **Fig. 4**, the radius of pillar and plate thickness are fixed as $r/a = 0.42$ and $e/a = 0.2$. The pillar height considered is $h/a = 0.6,\ 1.2,\ 1.8$. For $h/a = 0.6$, the low-frequency hybridization BG and broad Bragg BG is identical to the case discussed above, see **Fig. 3**. However, for $h/a = 1.2$, the lower BG seems to be closed and the central frequency of the higher BG shifts to a lower frequency spectrum. Likewise, for $h/a = 1.8$, the central frequency of the first two BGs shifts towards a lower frequency whereas a new BG at a higher frequency region is also witnessed. From the band structures shown in **Fig. 4**, it is observed that for few BGs, their opening is caused by the crossing of normal acoustic branches with highly localized flat bands, that is an interesting and main mechanism of local resonance phenomena.

Finally, the effect of different combinations of materials constituting pillars and plate on the robustness and persistence of subwavelength BG is also investigated. Five different materials (steel, tungsten, silicon, epoxy and aluminum) with different acoustic properties are considered. The plate and pillar materials are varied separately for investigating their effect on the low-frequency BG. In **Fig. 5**(a), the limit of low-frequency BG by varying the plate material is shown where the pillar is made of steel. Likewise **Fig. 5**(b) shows the BG limit for various pillar materials while the plate is made of silicon. The persistence of local resonance BG even with identical pillar and plate material can be observed. This further affirms the assertion that the hybridization BG is related to geometrical configuration of pillar-plate structure rather than the constituent materials. However, the central

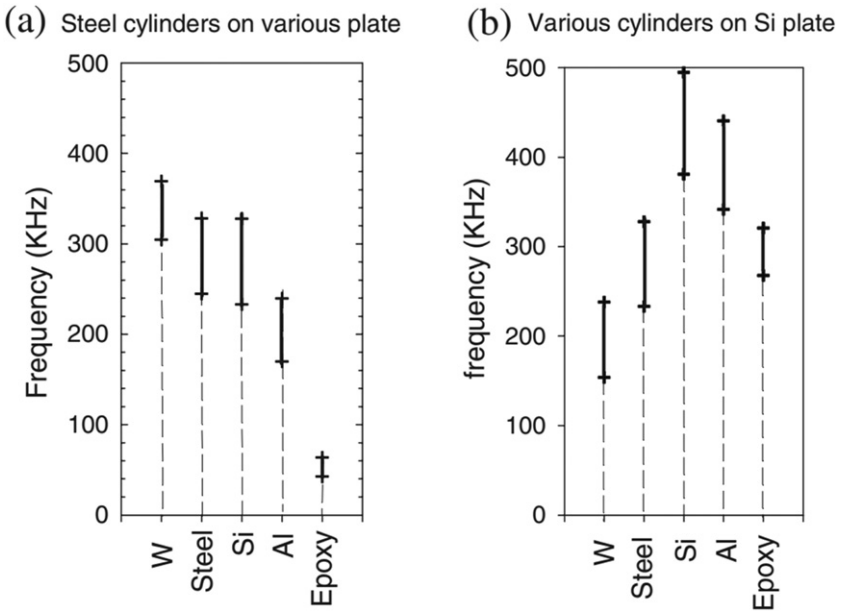

Fig. 5 Evolution of subwavelength locally resonant BG limits for different combinations of pillar and plate constituent materials. (a) Steel dots on a plate of different materials (b) multiple dots on a silicone plate. Reproduced with permission from Pennec, Y., Djafari-Rouhani, B., Larabi, H., *et al.*, 2008. Low-frequency gaps in a phononic crystal constituted of cylindrical dots deposited on a thin homogeneous plate. Physical Review B 78 (10), 1–8. 2008, APS.

frequency of BG does depends upon the constituent material and the BG shifts to a lower frequency region when high-density pillar material like steel or tungsten pillars is embedded on low-density plate material like epoxy. A correct choice of pillar-plate geometric parameters and constituent materials can generate extremely low frequency BG in order to control vibration and noise for high precision mechanical systems.

Wave Transmission and Waveguiding

The wave dispersion study performed in the prior section is based on Floquet-Bloch periodicity condition that presumes an infinitely periodic phononic pillar system. However, practically all "periodic" structures are of finite dimension. To envisage A0 and S0 Lamb waves propagation and attenuation inside a finite array of phononic lattice, a comprehensive study on wave transmission is of fundamental importance. In such a finite length model, the harmonic excitation source is placed at one end while displacement response is recorded at the opposite end. The response can be depicted in the form of transmission coefficient or wave transmissibility. Here we adopted the later approach to demonstrate propagation and attenuation of elastic Lamb waves in the pillar plate system. Apart from comparing wave transmission with a dispersion plot of pillared phononic crystal plate, the phenomena of waveguiding by removing one row of pillar is also presented. The ability to tune acoustic or elastic waves characteristics, especially for waveguides, makes such phononic system ideal for a wide range of applications, from transducer technology to acoustic/elastic wave guiding and filtering.

Fig. 6 shows the wave transmission behavior of pillared PnC plate that is made of a square array of steel pillars embedded on a thin homogenous elastic silicon plate. For better comparison, the band structure is depicted in the middle panel i.e., Fig. 6(b) and the A_0 and S_0 Lamb waves transmission plots are shown aside. The transmission spectra are computed in the $\Gamma - X$ direction of the irreducible Brillouin zone. Propagation of elastic waves in the passband and attenuation in BG frequency regions can be observed.

Next, we investigate the possibility to pass both S_0 and A_0 Lamb waves across a finite setup of pillared PnC plate by removing a row of pillars, as shown in Fig. 7(a). The system is excited by both types of Lamb wave separately and wave transmission curve is calculated. The length of waveguide is $10a$ and it is separated by 4 lines of solid steel pillar so that the coupling effect and leakage could be minimized. For better comparison, wave transmission for a perfectly periodic array of pillars is also given in Fig. 7(b) for both S_0 and A_0 Lamb waves. The energy of elastic waves can be localized inside the waveguide provided that the propagating wavelength lies inside the BG of perfectly periodic pillars. From Fig. 7(c) one can observe that at a higher frequency for both S_0 and A_0 Lamb waves when the passband is inside the BG region, robust elastic wave propagation across waveguide is observed. At low frequency region, the transmission of waves across waveguide is observed for S_0 Lamb wave while for A_0 Lamb wave, this effect is quite weak. To better illustrate the waveguiding effect inside BG, we show the propagation of both S_0 and A_0 Lamb monochromatic waves at the frequency of 1.915 MHz, 1.96 MHz and 2.63 MHz for S_0 Lamb wave and 0.84 MHz, 1.955 MHz and 2.105 MHz for A_0 Lamb wave.

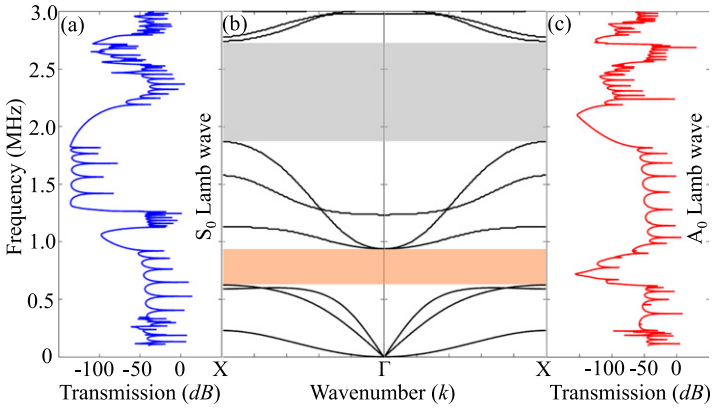

Fig. 6 (a, c) wave transmission for S_0 and A_0 Lamb waves propagating across a finite length square lattice arrangement steel pillars deposited on silicon plate. The geometric parameters adopted are: $h/a = 0.6$, $r/a = 0.42$ and $e/a = 0.2$. (b) wave dispersion curve calculated in the $\Gamma - X$ direction of the irreducible Brillouin zone. The figure is based on the results reported in Pennec *et al.* Reproduced from Pennec, Y., Djafari Rouhani, B., Larabi, H., *et al.*, 2009. Phonon transport and waveguiding in a phononic crystal made up of cylindrical dots on a thin homogeneous plate. Physical Review B 80 (14), 144302.

Temperature Biosensor Based on Pillared Phononic System

Like many other applications, PnC lattice can be applied as temperature biosensors to detect certain chemical like Methyl Nonafluorobutyl Ether (MNE), an organic mild solvent solution widely used in beauty products and cosmetics. The working mechanism is similar to PnC waveguiding principle discussed in the prior section. Recently, Zaremanesh *et al.* (2021) proposed a line of hollow pillars filled with MNE as a waveguide for directing the resonant modes with low group velocity into PnC biosensor which is comprised of a triangular lattice of tungsten pillars deposited in an epoxy substrate. The proposed PnC biosensor exhibits sharp transmission peaks indicative of localized modes in the BG frequency region with excellent quality factors and frequencies that are dependent on MNE temperature with great sensitivity. The 2D lattice structure with localized frequencies can perform temperature sensing to detect MNE in the temperature range from 10°C to 40°C. The presence of damping inside the liquid demonstrates that shear viscosity has a significant impact on the magnitude of resonant peaks when compared to longitudinal viscosity. Detection of temperature variations in MNE represents enormous applications for its wide daily use like in the cosmetic and beauty products due to non-flammable, non-toxic and colorless chemical properties.

To envisage the waveguiding effect by the proposed PnC triangular lattice, an array of 7×1 unit cell structure is considered and a hollow pillar with radius $r_i = 0.22a$ is inserted as shown in **Fig. 8**. The periodicity condition is applied at all edges of the supercell structure and by performing a wave dispersion study, the band structure for supercell lattice is obtained. The dispersion plot indicates the presence of a localized passband around 1 MHz that is present in the middle of a large phononic BG. Further, the wave transmission curve obtained shows the presence of sharp transmission peak at the localized passband frequency, see **Fig. 8**. By analyzing displacement field, the localization of wave energy inside the hollow tungsten pillar can be observed. The frequency of these modes can be tailored by varying the inner radius r_i of hollow phononic pillar in the triangular lattice system. Such localized cavity mode can be of high interest for telecommunication applications. A detailed analysis on this type of modes for hollow phononic pillars is given in Section "Whispering Gallery Modes of the Hollow Phononic Pillars".

Next the hollow pillar is filled with MNE liquid and likewise a wave dispersion study is performed on the supercell structure, as shown in **Fig. 9**. The properties of MNE considered are: sound velocity $v_{MNE} = 650.5m/\text{sec}$ and density $\rho_{MNE} = 1554\text{kg}/m^3$. The temperature of MNE is assumed as 10°C. The band structure shows the presence of two additional flat bands (B and C) inside the BG frequency region that are present above and below the localized band A. The displacement fields for these bands are shown in **Fig. 9**(b) where the distribution of acoustic energy is depicted. By varying temperature of MNE from 10°C to 40°C, the acoustic energy localization can be tailored inside the BG frequency range. Interested readers are referred to Zaremanesh *et al.* (2021) for more detailed insights.

Surface Acoustic Wave Propagation in Pillared Phononic System

This section will investigate the methodology to generate surface acoustic wave (SAW) and study their propagation behavior across the pillared PnC and AM systems. Compare to Lamb wave that propagates in thin elastic plate system, the replacement of wave propagating medium (thin plate) with semi-infinite half-space alters the wave phenomena and it results in novel effect that is not observed in both S_0 and A_0 Lamb waves. This section will also present an analysis on SAW band structure while the fundamental modes of phononic pillars responsible for opening BG will be discussed. An insight on the finite length model will be given to generate SAW and observe their propagation behavior upon interaction with a finite array of phononic pillar system.

The schematic diagram for a unit cell structure that consists of pillar structure deposited on the surface of a semi-infinite half-space is shown in **Fig. 10**(a). The finite length model for SAW generation and propagation with a finite array of pillars is shown in **Fig. 10**(b). Here we consider crystalline silicon as both pillar and substrate material with mechanical properties $C_{11} = 166\text{GPa}$, $C_{12} = 64\text{GPa}$, $C_{44} = 79.6\text{GPa}$ and mass density $\rho = 2330\text{kg}/m^3$. To focus on the propagation and interaction of surface waves with phononic pillars and to investigate their

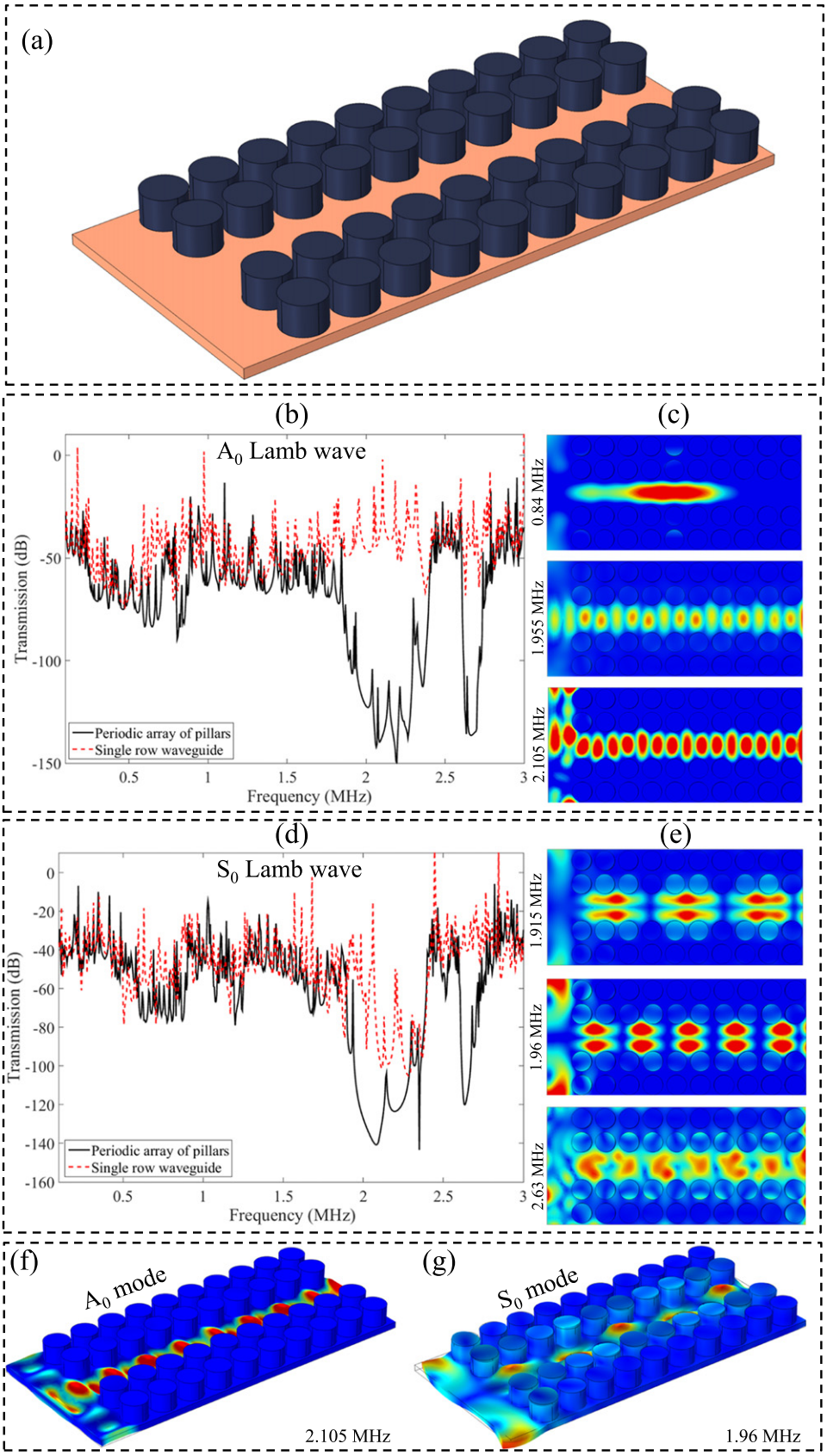

Fig. 7 (a) Schematic diagram of a single row line defect waveguide with pillar height and radius $h/a = 0.6$, $r/a = 0.42$ and plate thickness $e/a = 0.2$. (b,c) A_0 Lamb wave transmission curve, and (d,e) S_0 Lamb wave transmission curve through perfectly periodic phononic pillars and line-defect waveguide. The displacement field plots for some frequencies are also depicted. (f,g) 3D view of displacement field plot for A_0 and S_0 wave modes with localized energy propagating across the single row waveguide.

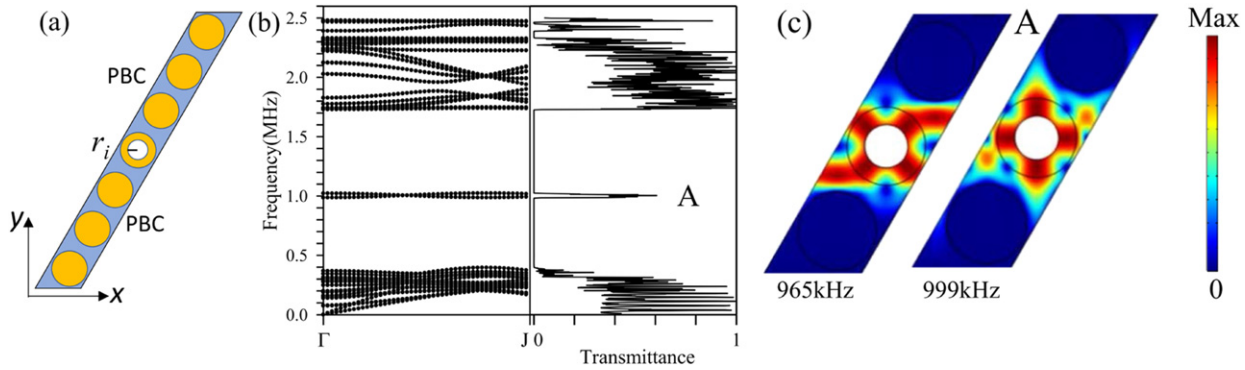

Fig. 8 (a) Pillared PnC triangular supercell structure where a hollow tungsten pillar with inner radius $r_i = 0.22a$ is embedded. The periodicity condition is applied on all edges. (b) Wave dispersion and transmission curve obtained by performing wave dispersion and frequency response studies, respectively. The localized mode A with (c) displacement fields can be seen where wave energy is completely localized inside the hollow phononic pillar. The figure is based on the results reported in Zaremanesh *et al.* Reproduced from Zaremanesh, M., Carpentier, L., Gharibi, H., *et al.*, 2021. Temperature biosensor based on triangular lattice phononic crystals. APL Materials 9 (6), 061114.

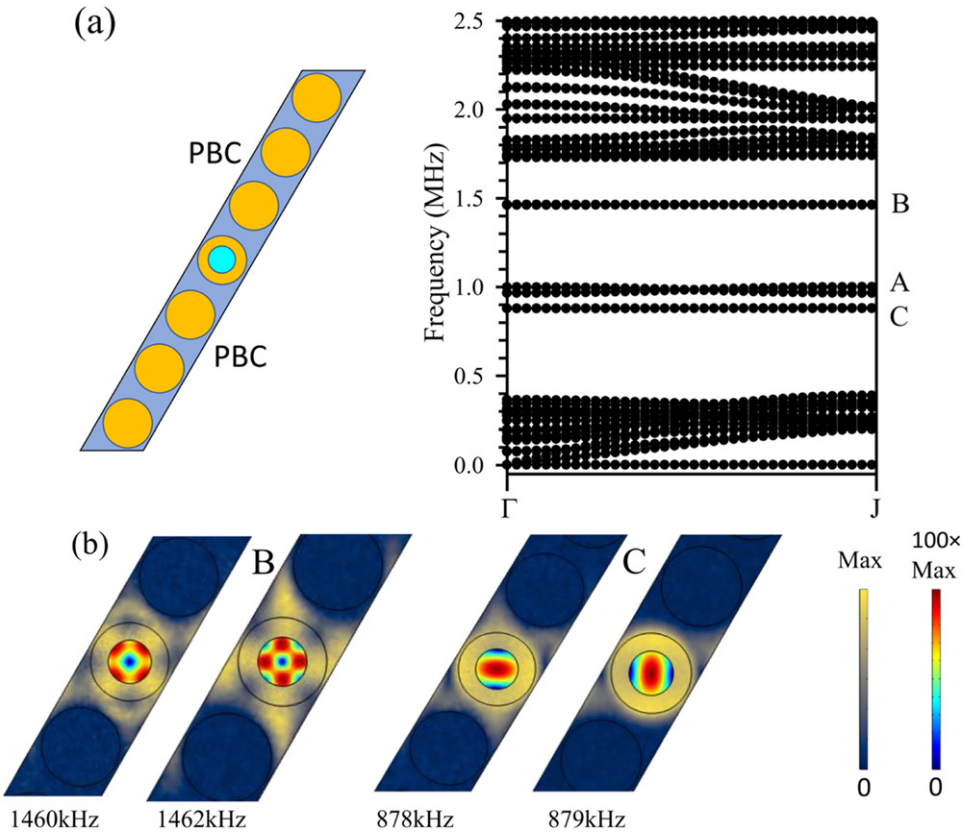

Fig. 9 (a) Representation of the pillared phononic supercell structure when the hollow pillar is filled with MNE at 10°C and the corresponding band structure with localized flat bands. The periodicity condition is applied on all edges of the unit cell structure. (b) The displacement field distribution in the solid and liquid region for localized mode B and C. The displacement field bar for solid and liquid are shown on left and right, respectively. The figure is based on the results reported in Zaremanesh *et al.* Reproduced from Reproduced from Zaremanesh, M., Carpentier, L., Gharibi, H., *et al.*, 2021. Temperature biosensor based on triangular lattice phononic crystals. APL Materials 9 (6), 061114.

dynamical characteristics, the material is assumed as homogenous, linear elastic and isotropic. For further details about theory, governing equations and mathematical formulation, one can refer to Muhammad *et al.* (2019a); Muhammad *et al.* (2020). The governing eigenvalue equation is solved by using finite element code COMSOL Multiphysics.

Fig. 11 shows the SAW band structure for a unit cell model shown in Fig. 10(a). The Floquet-Bloch periodicity condition is applied on all the vertical edges. The bottom of the unit cell structure is fixed while the top surface is traction free. The wave

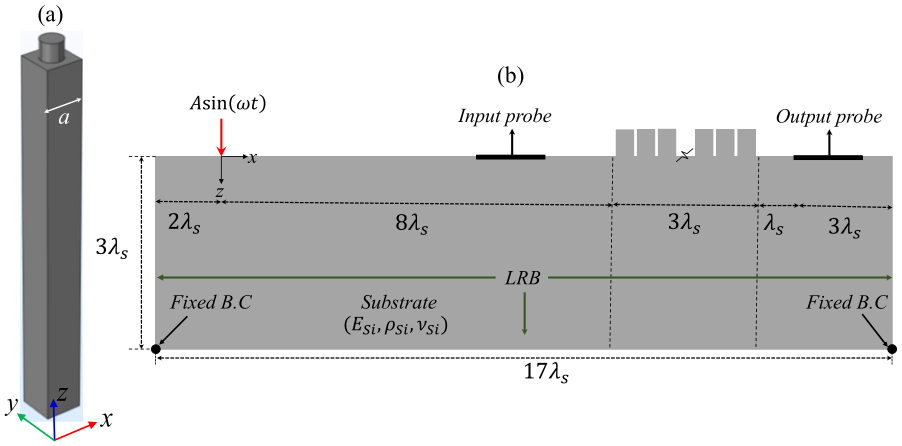

Fig. 10 (a) unit cell structure (b) finite length model constructed to investigate SAW propagation across a periodic array of pillars. The figure is based on the results reported in Muhammad Reproduced from Muhammad, 2021. Dynamic Characteristics of Phononic Metamaterials with Amplified Bandgaps for Wave Manipulation and Seismic Shielding Applications. City University of Hong Kong.

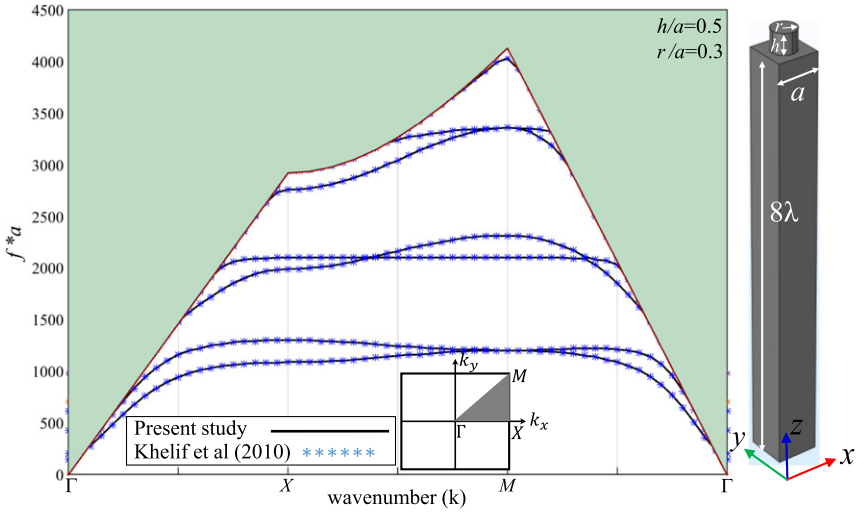

Fig. 11 SAW band structure for crystalline silicon pillar PnC deposited on the surface of silicone semi-infinite half-space. The figure is based on the results reported in Khelif *et al.* and Muhammad *et al.* Reproduced from Khelif, A., Achaoui, Y., Benchabane, S., *et al.*, 2010. Locally resonant surface acoustic wave band gaps in a two-dimensional phononic crystal of pillars on a surface. Physical Review B 81 (21), 1–7. Muhammad, Lim, C.W., Reddy, J.N., et al., 2020. Surface elastic waves whispering gallery modes based subwavelength tunable waveguide and cavity modes of the phononic crystals. Mechanics of Advanced Materials and Structures 27 (13), 1053–1064.

dispersion analysis usually shows the presence of bulk wave, shear wave, leaky surface wave, SAW modes, etc. In this section all result is presented in the form of reduced frequency $f * a$. To separate SAW modes from other bulk wave modes, the band structure is plotted by using the sound cone technique which is an efficient method that separates SAW modes from other spurious bulk modes. This method distinguishes different wave modes based on the phase velocity of a particular resonant mode, dividing the band structure of a phononic periodic system into two components, termed as radiative and non-radiative wave regions. Here, the word radiation refers to the penetration of wave energy from the surface of half-space deep into the substrate. These two regions are separated by the sound line. For this purpose, it is deemed appropriate to develop a program in MATLAB to generate this sound line. Mathematically, the bounding velocity of the sound line can be expressed as $\omega = \mathbf{k}c_s$ where $c_s = \sqrt{\mu/\rho}$ and c_s, μ, ρ are shear wave velocity, shear modulus and mass density of silicon crystal, respectively. All resonant modes that lie below the sound line possess wave velocity smaller than c_s and such eigenmodes are surface wave modes with wave energy concentrated at the free surface of phononic pillar with decaying energy field going deep into the semi-infinite substrate. Those eigenmodes are present in the non-radiative region of a wave dispersion plot. Likewise, the resonant modes with wave speed larger than c_s have wave energy that concentrates into the semi-infinite substrate, and not at the surface. These high speed eigenmodes are placed inside the radiative region. In this way the surface wave eigenmodes are separated from other bulk or mixed wave modes, which are outside of the research area of this study.

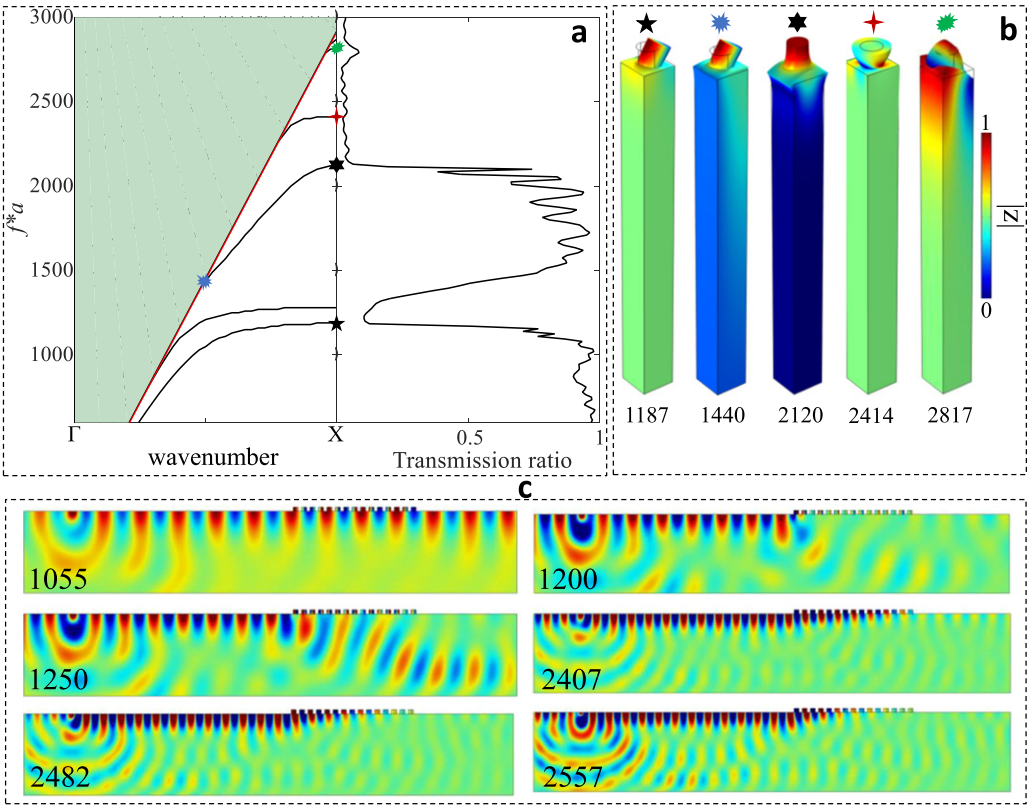

Fig. 12 Band structure with SAW transmission curve for solid silicon pillar with $r/a = 0.3$ and $h/a = 0.5$ deposited on the surface of semi-infinite substrate, (b) vibration modes responsible for BG generation, and (c) displacement field plots for passband and BG frequencies. The figure is based on the results reported in Muhammad. Muhammad, 2021. Dynamic Characteristics of Phononic Metamaterials with Amplified Bandgaps for Wave Manipulation and Seismic Shielding Applications. City University of Hong Kong.

To envisage surface wave propagation and investigate their interaction with resonant pillars, a finite length model has been adopted, see **Fig. 10**(b). All geometric parameters are represented with reference to λ_s to ensure the propagation of all frequencies through all mesh elements. This is frequently established by selecting the maximum frequency. To ensure more accurate computations, at least five mesh elements per wavelength are embodied during the meshing process. To avoid back-reflection of spurious bulk waves from both ends and bottom boundaries, the low reflection boundary (LRB) condition is applied (Muhammad *et al.*, 2021c). The LRB avoids back-reflection of incident waves from boundaries of the finite length model and ensures propagation of SAW on the top surface of substrate. An equal length input probe and another output probe are set to measure the associated vertical displacement fields. SAW is generated by applying harmonic excitation at distance $8\lambda_s$ away from the periodic array of phononic pillars. In such finite length setup, SAW propagates at the free-surface with decaying energy field deep into the substrate.

Following the methodology described above, a frequency response study on the finite length model is performed. From **Fig. 12** one can observe the propagation and attenuation of SAW inside passband and BG frequency regions, respectively. The frequency response study is performed in the $\Gamma - X$ direction of the irreducible Brillouin zone and it is compared with the frequency response spectrum. The resonant modes are also highlighted in **Fig. 12**(b) and we found that the longitudinal resonant mode (third fundamental mode) is majorly responsible in opening the BG. This is due to the hybridization of elliptically polarized SAW with vertical ground motion and longitudinal resonant mode of the phononic pillar. Likewise, the first two resonant modes also open a narrow local resonance BG in the frequency range 1187–1140 Hz. The fourth and fifth resonant modes are torsional and mixed modes, which cause a limited effect on local resonance BG. The displacement field plots for passband and BG frequencies are presented in **Fig. 12**(c). The attenuation of SAW upon interaction with pillar structures can be observed in the BG frequency region.

Whispering Gallery Modes of the Hollow Phononic Pillars

This section will put forward a brief insight on the localized cavity modes of hollow phononic pillars, the so-called whispering gallery modes (WGMs) subjected to A_0 Lamb wave (for phononic pillars embedded on thin-place) and SAWs (an array of phononic pillars are deposited on the semi-infinite substrate). A detailed analysis of the models is given in the prior sections. This section will mainly focus on the WGMs of hollow phononic pillars. Before going into further details, a general understanding of WGM is necessary to

grasp the discussion in the next sections. The initial work on WGMs can be related to early 1910 when Rayleigh studied sound wave propagation around St. Paul's Cathedral gallery (Rayleigh, 1910). Since then multiple studies were reported and the capabilities of WGMs resonators for wave modulation (Peng *et al.*, 2014), sensing (Foreman *et al.*, 2015) and filtering (Li *et al.*, 2013) applications were explored in photonics and wave optics. Like other resonators, a hollow pillar structure can also introduce WGMs and the quality factor can be increased by introducing another solid pillar at the bottom of hollow pillar. By adjusting the geometric parameters the frequency of localized cavity mode can be tuned. In this section we consider silicon hollow pillars with a square lattice arrangement deposited on silicon plate and semi-infinite substrate, as explained in the prior section. Some parts of the results discussed in the following sections are reproduced from Jin *et al.* (2016a) and Muhammad *et al.* (2020).

Hollow Phononic Pillars Subjected to Lamb Waves

First the band structure for a standard solid pillar with geometric parameters $h/a = 0.45$, $r/a = 0.4$ and plate thickness $e/a = 0.1$ is presented, see **Fig. 13**(a). The band structure is reminiscent to findings reported in the prior sections. As explained above, one can observe the presence of both Bragg and hybridization/local resonance BGs simultaneously and hence such pillared phononic structure can be perceived to work as PnC and AM. Next, we drill a hole with an inner radius $r_i/a = 0.145$ and perform a wave dispersion study as shown in **Fig. 13**(b). Introducing a hollow pillar gives birth to two new bands that are marked as WGM(i) and WGM(ii). Similarly, a wave transmission study is conducted and the result reported in **Fig. 13**(c) indicates that WGM(ii) is a deaf mode and only wave transmission peak is observed for WGM(i). Both quadrupolar WGMs are shown in **Fig. 13**(d). The displacement field plots indicate that WGM(ii) is symmetric with respect to the *x*-*z* plane, therefore it is compatible with symmetry of incident A_0 Lamb wave, thus it can be excited. In contrast, WGM(i) is asymmetric and therefore we did not observe any transmission peak and it can be perceived as a deaf mode. Further, it is interesting to note that the quality factor of WGM(i) can be increased by sandwiching a solid pillar between the hollow pillar and the plate. Further details of the analysis can be found in Jin *et al.* (2016a).

For a given WGM(i), the acoustic route of WGM around the hollow phononic pillar is a multiple integer of the wavelength equal to 2. As a result, the wavelength has a qualitative behavior as $\langle r \rangle = (r + r_i)/2$. If the radius of hollow pillar is further increased, it shifts WGMs to a subwavelength frequency region, in the vicinity of the local resonance BG. Therefore, by varying the inner radius of hollow pillar, WGMs can be tuned. Further details can be found in Jin *et al.* (2016a).

A further insight on the localized cavity modes (WGMs) on the band structure is depicted in **Fig. 14** where we change the inner radius of hollow pillars to locate the position of WGMs. It can be seen that when the inner radius of hollow pillar is increased, the localized cavity modes i.e., WGM(i) and WGM(ii) shift to a lower frequency region. Therefore, an appropriate choice of r_i/a can position the localized modes inside the hybridization BG at the subwavelength frequency regime. Such a strategy may result in promising findings for subwavelength waveguiding and focusing applications in photonic and phononic systems.

Next, we demonstrate the propagation of A_0 Lamb wave through a multichannel wavelength multiplexer that consists of a 5×5 array of pillar structures deposited on a thin plate. The setup consists of an array of solid pillar with hollow pillars of radii $r_i/a^{(a)} = 0.145$ and $r_i/a^{(a)} = 0.16$ running parallelly. The wave transmission and displacement field plots are shown in **Fig. 15** where the transmission peaks for WGMs are presented alphabetically. One can observe the propagation of waves in the designated path at the transmission peak frequency (that actually excites WGMs of hollow pillars) and wave isolation is observed in the neighboring solid pillar structures. Similar effects can be envisaged for monochannel and compact channel waveguides as reported in Jin *et al.* (2016a). Such WGMs of hollow pillars may have promising applications in wave filtration, wavelength multiplexing and sensing applications.

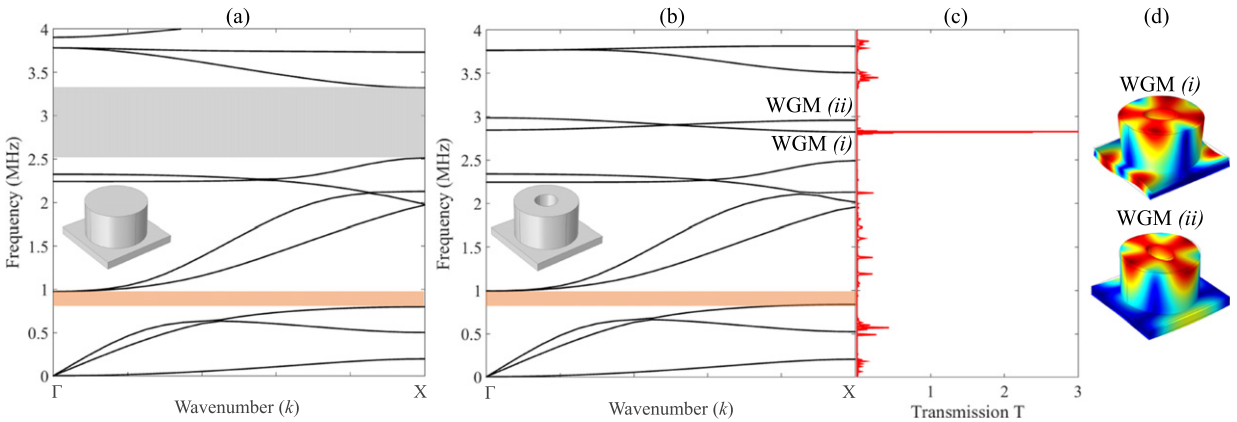

Fig. 13 Wave dispersion for (a) solid pillar (b) hollow pillar deposited on a thin elastic plate in the direction of the irreducible Brillouin zone. The solid pillar geometric parameters are: . The inner radius of hollow pillar is and all other geometric parameters are identical. Hollow pillar introduces two new passband in the BG frequency range and (c) the wave transmission curve shows the presence of transmission peak corresponding to WGM(i) when excited by an incoming A0 Lamb wave (d) the WGM(i) and WGM(ii). The figure is based on the results reported in Jin *et al.* Reproduced from Jin, Y., Fernez, N., Pennec, Y., *et al.*, 2016a. Tunable waveguide and cavity in a phononic crystal plate by controlling whispering-gallery modes in hollow pillars. Physical Review B 93 (5), 054109.

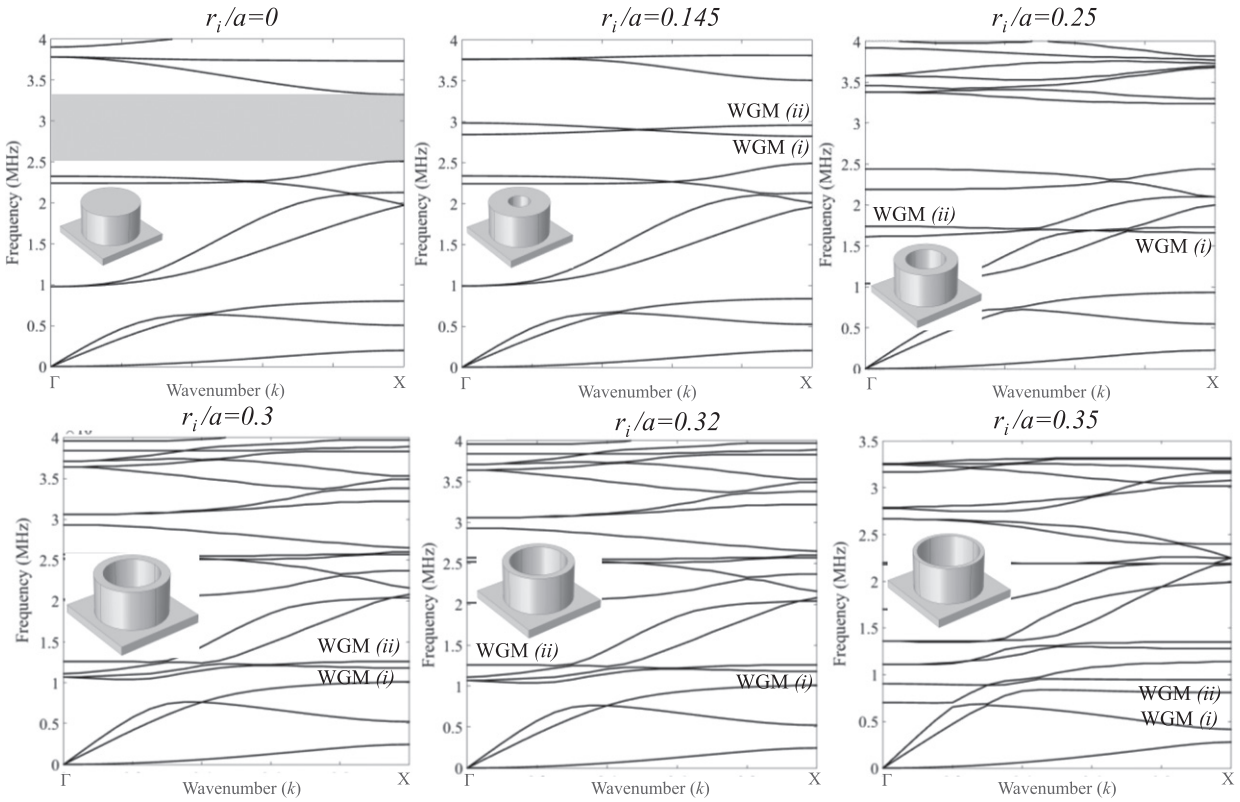

Fig. 14 Band structure of hollow phononic pillar with inner radii $h/a = 0$, 0.145, 0.25, 0.3, 0.32, 0.35 deposited on silicon plate in the $\Gamma - X$ direction of the irreducible Brillouin zone. WGMs are highlighted and schematic diagram of hollow pillar is shown at the inset of wave dispersion plot. The figure is based on the results reported in Jin *et al.* Reproduced from Jin, Y., Fernez, N., Pennec, Y., *et al.*, 2016a. Tunable waveguide and cavity in a phononic crystal plate by controlling whispering-gallery modes in hollow pillars. Physical Review B 93 (5), 054109.

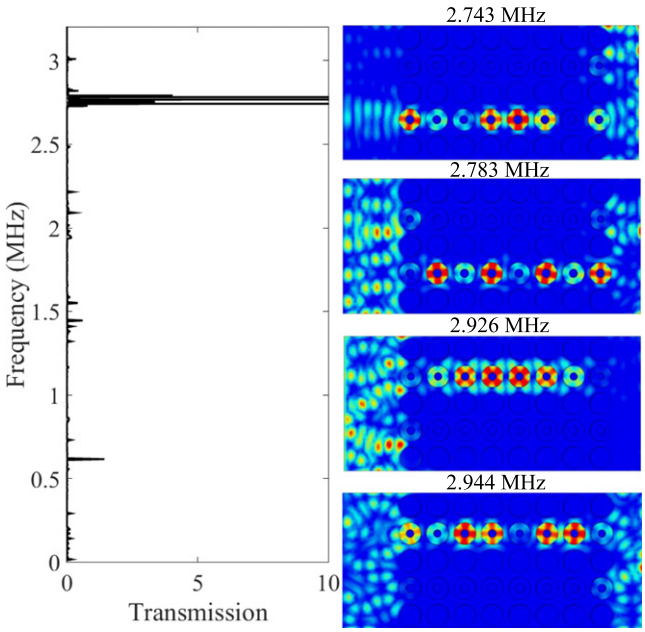

Fig. 15 Applications of WGM*(i)* in a multichannel waveguide with inner radii of hollow pillars $r_i/a = 0.145$ and $r_i/a = 0.16$. At localized cavity mode frequencies presented in the wave transmission curve, propagation of A_0 Lamb wave across the waveguide can be seen. The figure is based on the results reported in Jin *et al.* Reproduced from Jin, Y., Fernez, N., Pennec, Y., *et al.*, 2016a. Tunable waveguide and cavity in a phononic crystal plate by controlling whispering-gallery modes in hollow pillars. Physical Review B 93 (5), 054109.

Hollow Phononic Pillars Subjected to SAWs

We discussed SAW propagation and interaction with pillared structures in Section "Temperature Biosensor Based on Pillared Phononic System". This section extends the analysis to WGMs of hollow phononic pillars when subjected to SAWs. The material properties are identical to the prior section where both pillar and substrate are made of crystalline silicon. The result is presented in the form of reduced frequency $f * a$ where f is general frequency and a is periodicity constant. As discussed in Section "Hollow Phononic Pillars Subjected to Lamb Waves", to investigate WGMs of hollow phononic pillars, a solid phononic pillar is replaced with a hollow pillar. Reminiscent to Fig. 14, the evaluation of band structures for varying hollow pillar is carried out in Fig. 16. It has been identified that the presence of hole introduced four additional Bloch bands that are labeled as 1–4 for different frequencies. Because these modes are absent in the solid pillar, therefore we refer them as localized cavity modes or WGMs of hollow pillars. Further, these modes are generated due to the interaction of SAWs with hollow phononic pillars. From Fig. 16 one can observe that with increasing inner radius r_i, WGMs move towards a lower frequency region. For instance, for $r_i/a = 0.173$, the WGMs 1–2 appear inside the second BG and for $r_i/a = 0.233$, these localized cavity modes shift towards the first BG. For $r_i/a = 0.241$, WGM 2 remains inside the first BG, while WGMs 3–4 appear inside the second BG.

The filtering capacity of WGMs is demonstrated that employs a finite unit cell based wave transmission study. The schematic diagram for a finite length model adopted is showcased in Fig. 10. The wave transmission is computed as $T = (w_{out}/w_{in})^2$ where w_{out} and w_{in} are the integration of displacement fields at the output and input probes, respectively. A periodic continuity condition is maintained along the y-direction on both sides of the finite length model, in order to reduce the numerical computational effort. In Fig. 17, the wave transmission response for a periodic array of hollow pillars with $r_i/a = 0.233$ is presented to study the presence

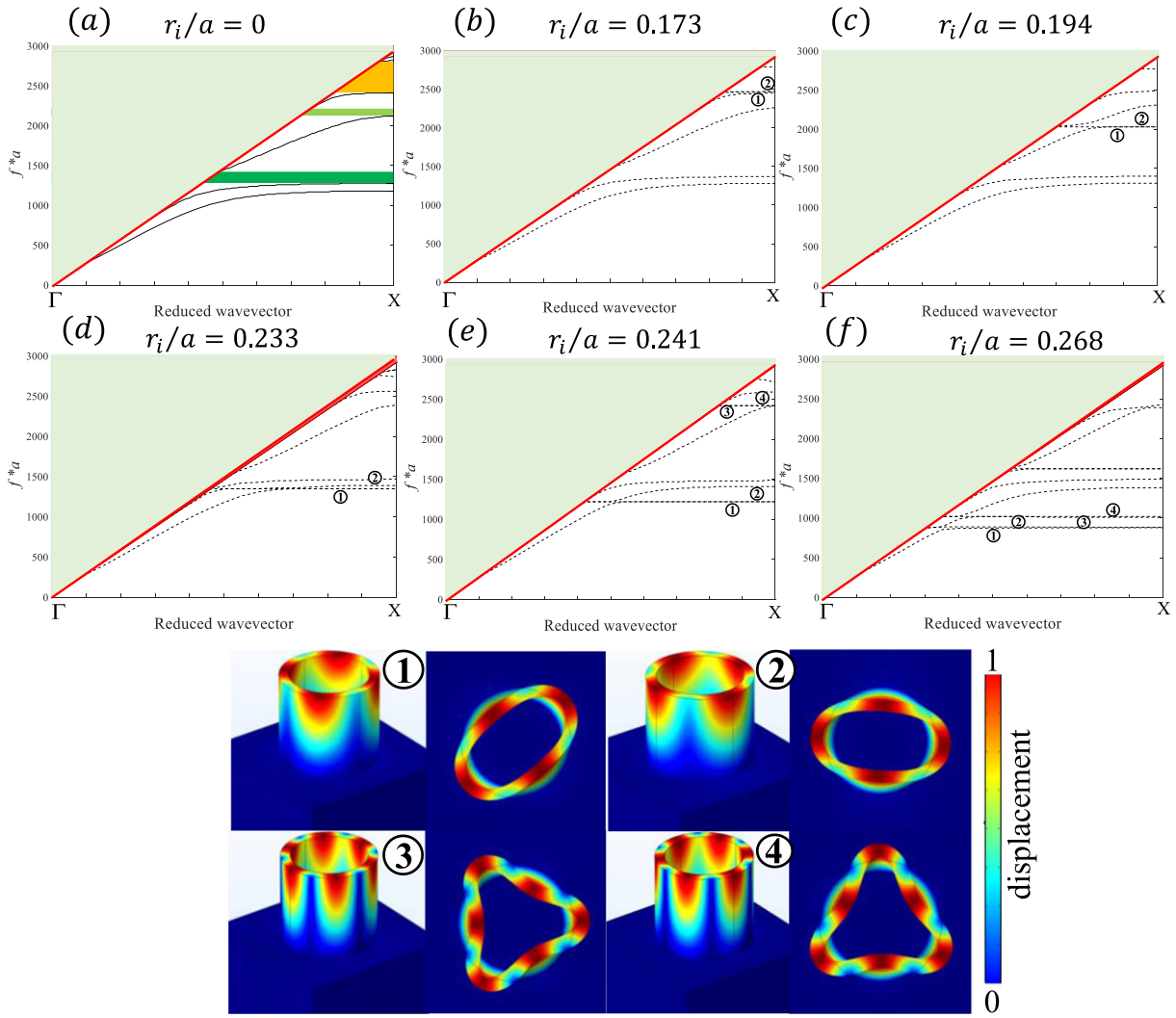

Fig. 16 Band structures of hollow phononic pillars deposited on the surface of semi-infinite half-space in the $\Gamma - X$ direction of the Brillouin zone with varying inner radius. The outer radius is $r/a = 0.3$. The WGMs of SAW modes are shown at the bottom row. The figure is based on the results reported in Muhammad *et al.* Reproduced from Muhammad, Lim, C.W., Reddy, J.N., *et al.*, 2020. Surface elastic waves whispering gallery modes based subwavelength tunable waveguide and cavity modes of the phononic crystals. Mechanics of Advanced Materials and Structures 27 (13), 1053–1064.

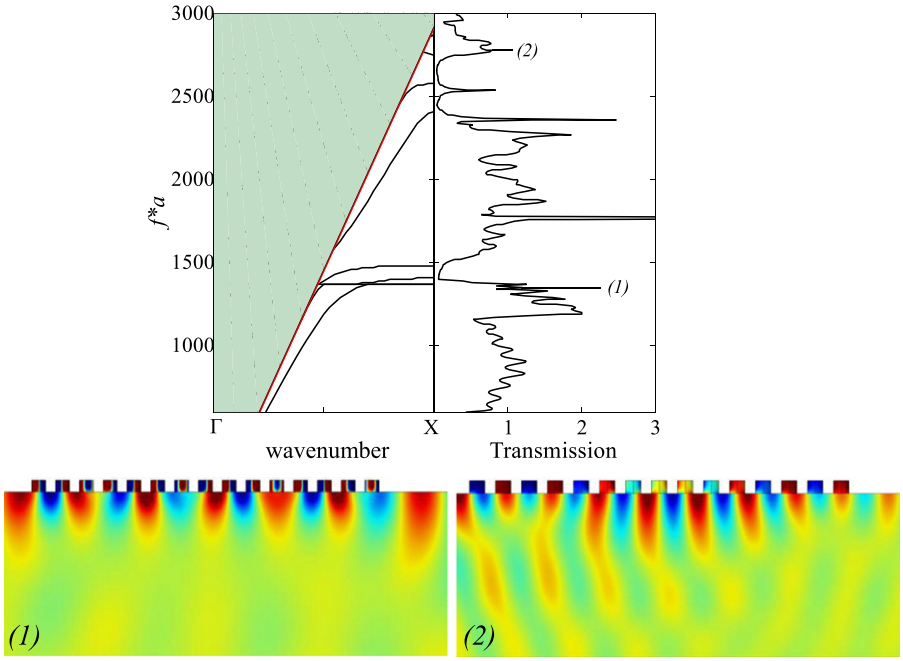

Fig. 17 (*top row*) Band structure with wave transmission of the hollow phononic pillar with $r_i/a = 0.233$. Points (*1*) and (*2*) are WGMs of the hollow pillars with high energy transmission. (*bottom row*) Out-of-plane displacement field at WGM frequencies. The figure is based on the results reported in Muhammad. Reproduced from Muhammad, 2021. Dynamic Characteristics of Phononic Metamaterials with Amplified Bandgaps for Wave Manipulation and Seismic Shielding Applications. City University of Hong Kong.

of passband for SAW propagation inside the BG of solid phononic pillar. The displacement field plots for WGM frequencies are captured and high surface wave transmission at the surface of semi-infinite half-space can be observed in **Fig. 17** (bottom row). For BG frequencies, one can imagine identical SAW wave attenuation as depicted in the displacement field in **Fig. 12**. Further details can be found in Muhammad *et al.* (2020).

Next, an investigation on the subwavelength waveguiding characteristic by these confined cavity modes is performed. In such a waveguide, it is necessary for the localized Bloch band to lie inside the BG frequency region of solid phononic pillars. Under this condition, SAW cannot propagate in solid pillars while wave energy localization can be envisaged by hollow pillars. This effect is demonstrated in **Fig. 18** by considering an array of hollow pillar $r_i/a = 0.233$ that has parallelly running solid pillars in the neighborhood. The wave transmission curve indicates the presence of sharp transmission peaks that is associated with hollow cavity modes. From the displacement field plots, one can observe the localization of SAW energy in the hollow pillar with decaying energy fields in the solid pillars. This effect is also demonstrated by localizing wave energy in the abbreviation "ACE" which stands for "Architecture and Civil Engineering". At the localized frequency, the propagation of SAW along designated paths can be observed.

Resonances in Multilayer Phononic Pillars

This section puts forward an insight on PnCs that consists of multilayer pillars, stacked over each other for Lamb waves and SAWs manipulation. Each pillar is comprised of periodic stack of alternating layers as shown in **Fig. 19**. For the analysis in this section, the lattice constant is $a = 1$ mm and the PnC unit cell structure consist of silicon (Si) and tungsten (W) pillars where the Si pillar is sandwiched between two W pillars. The details for material and geometric parameters are given in Muhammad *et al.* (2021b). For a wave dispersion study, the Floquet–Bloch periodicity condition (PBC) is applied in the x-y-z directions, as observed in **Fig. 19**(b). The supercell model, constructed for the plane wave transmission curve/frequency response study, is shown in **Fig. 19**(c). It is commonly accepted, that in the case of such a periodic array the harmonic excitation is applied at the left end of the supercell model, and displacement fields are recorded at the opposite end. The displacement field is presented with respect to the frequency range of intertest to obtain the wave transmission curve. The transmission ratio is determined by taking the natural log of the ratio of output displacement fields (right end) to input displacement fields (left end). The wave transmission study provides information of a significant practical value, with regards to the wave propagation and attenuation at different passband and BG frequencies.

In **Fig. 20**, the wave dispersion response with BGs in the $x - y$ directions, i.e., $\Gamma XM\Gamma$; the z-direction i.e., $RXMR$ and the x-y-z direction is presented. Here BG is generated due to the coupling of a plane wave with local resonances of the PnC unit cell structure. At the BG opening edge, vibration is concentrated in the complete unit cell structure as depicted in **Fig. 20**(d). Therefore, it enhances the effective mass density and moment of inertia, further positioning the eigenfrequency to a relatively low frequency. At the closing

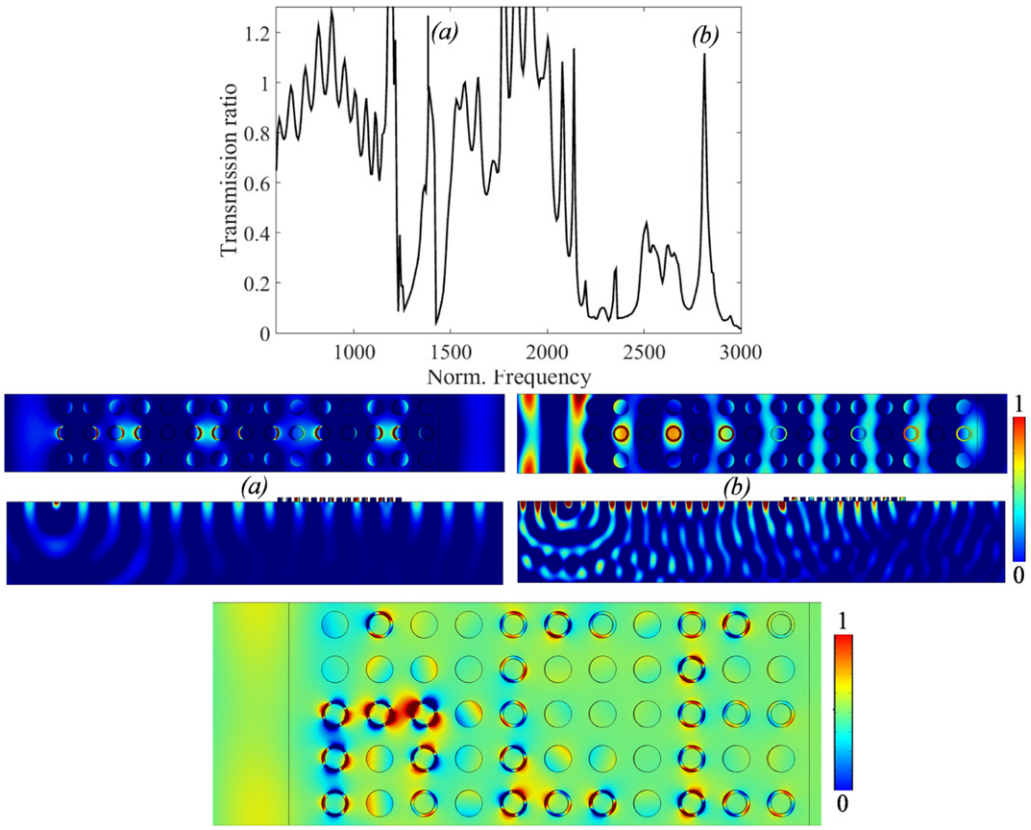

Fig. 18 Wave transmission spectrum of SAW propagating through hollow phononic pillars $r_i/a = 0.233$ waveguide bounded by parallel rows of two solid silicon pillars. The displacement field at reduced frequency $f * a = 1414$ and $f * a = 2518$ corresponding to point *(a, b)* respectively are shown at the bottom row. The SAW propagation in "ACE" that stands for "Architecture and Civil Engineering" can also be seen as an example of waveguiding and wave energy trapping phenomena. The figure is based on the results reported in Muhammad. Reproduced from Muhammad, 2021. Dynamic Characteristics of Phononic Metamaterials with Amplified Bandgaps for Wave Manipulation and Seismic Shielding Applications. City University of Hong Kong.

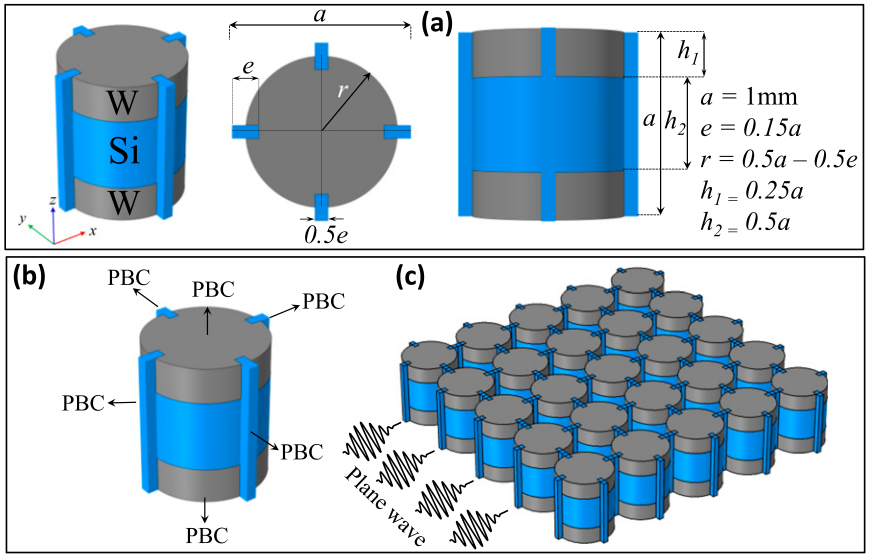

Fig. 19 The PnC unit cell structure and finite-length model: (a) 3D, top and plan view; (b) unit cell structure with periodic boundary condition (PBC) applied along all vertical edges, top and bottom; (c) supercell model used for plane wave transmission study. The figure is based on the results reported in Muhammad *et al.* Reproduced from Muhammad, Lim, C.W., Leung, A.Y.T., 2021b. Plane and surface acoustic waves manipulation by three-dimensional composite phononic pillars with 3D bandgap and defect Analysis. Acoustics 3 (1) 25–41.

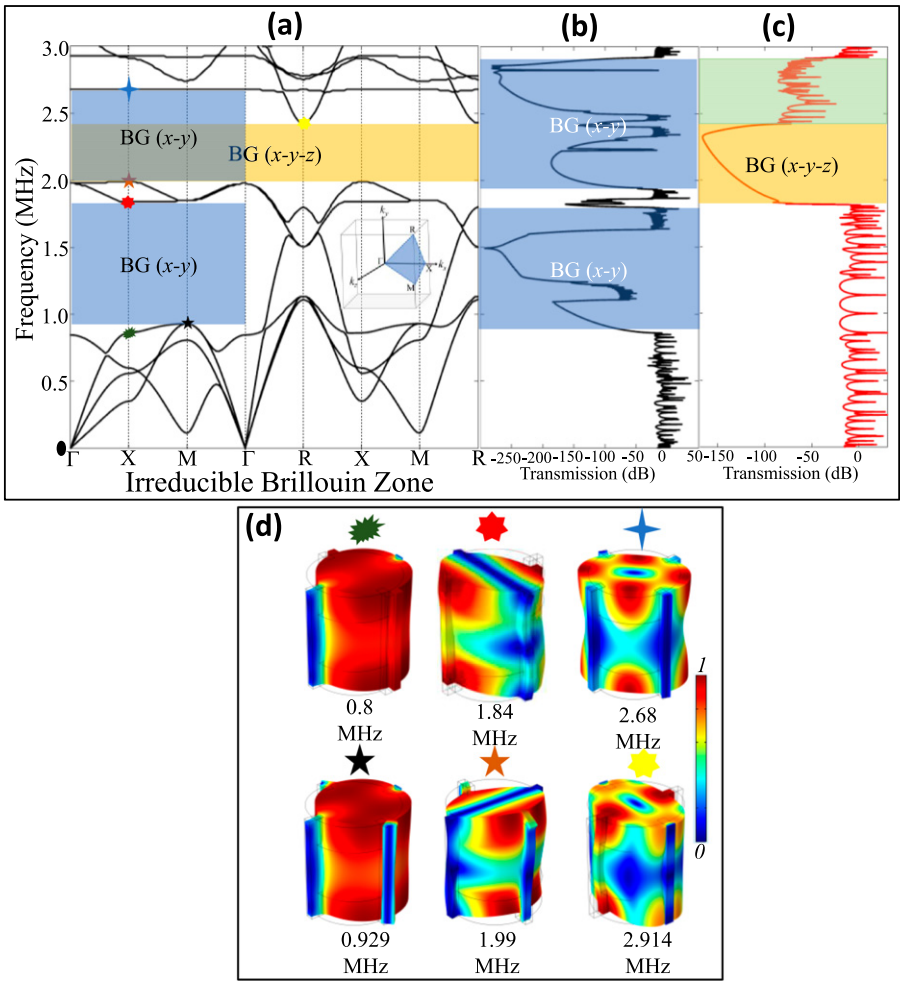

Fig. 20 (a) 3D band structure of PnC unit cell structure, with IBZ shown at the inset. (b-c) transmission curve for excitation in the x-y and the x-y-z directions. BGs are highlighted. (d) Vibration modes involved in the opening and closing of BGs. The figure is based on the result reported in Muhammad *et al.* Reproduced from Muhammad, Lim, C.W., Leung, A.Y.T., 2021b. Plane and surface acoustic waves manipulation by three-dimensional composite phononic pillars with 3D bandgap and defect Analysis. Acoustics 3 (1) 25–41.

bounding edge, the structure experiences flexural vibration, with distributed displacement fields/vibration energy concentrated at a few parts of the structure, causing the eigenfrequency to fall within a relatively higher frequency region. A similar trait can be seen across the boundary of IBZ for other points at $\Gamma XM\Gamma$ (first BG) and $\Gamma XM\Gamma RXMR$ (second BG) coordinates. These distinctions, caused by the local and global resonances of structure, result in the opening and closing of BG (Muhammad and Lim, 2021c,d).

Wave attenuation inside the BG frequency region is envisaged by constructing a finite number of unit cell structure and performing a frequency response study. For the wave transmission study in **Fig. 20**(b,c), the total displacement field in the *x-y-z* directions is captured in the frequency response spectrum plot. For the same reason, one can observe that in **Fig. 20**(c) half of BG ranging from 1.84 MHz to 2.68 MHz indicates an apparently clear plane wave attenuation. Nevertheless, response peaks above 2.68–2.9 MHz are observed. Although the response peaks exist and the BG curve is not smooth, the displacement field distribution in the supercell model indicates that it is the BG frequency region, which is responsible for wave attenuation in the supercell structure.

Next, we perform a defect analysis for in-plane elastic wave propagation across a finite array of unit cell structure. In **Fig. 21** a supercell structure with defect height h_d is shown. The finite length structure consists of seven unit cells with a defect state in-between. By performing a frequency response study, the vertical displacement field $|u_z|$ is calculated at the topmost layer. Wave transmission with defect states is depicted in **Fig. 21** where h_d is set as $0.05a, 0.1a, 0.15a$ and $0.2a$. For all cases considered, wave energy localization inside the defect and decaying energy field in the neighboring unit cell structures at the corresponding defect frequency is observed. Such an induced defect state may have promising applications in energy harvesting and sensing applications.

Multilayer pillars or ridge phononic structure can also be used to manipulate SAWs. To put forward an insight, here we refer to earlier studies reported by Oudich *et al.* (2018) where a periodic array of pillars as ridge structure is proposed as shown in **Fig. 22**(a). The phononic structure consists of two materials where the yellow layers are made of PMMA and blue pillars are silicon. Such type of pillar

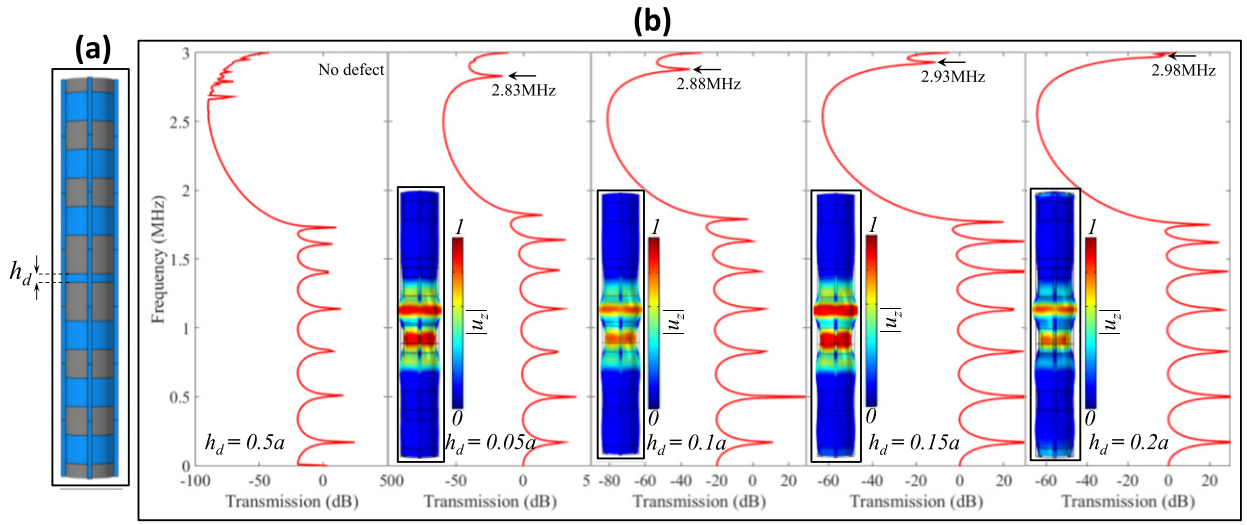

Fig. 21 Plane elastic wave defect analysis (a) supercell structure with defect height h_d (b) frequency response spectrum with defect frequency for varying h_d. Wave energy localization at the defect frequency can be observed. The figure is based on the result reported in Muhammad *et al.* Reproduced from Muhammad, Lim, C.W., Leung, A.Y.T., 2021b. Plane and surface acoustic waves manipulation by three-dimensional composite phononic pillars with 3D bandgap and defect Analysis. Acoustics 3 (1), 25–41.

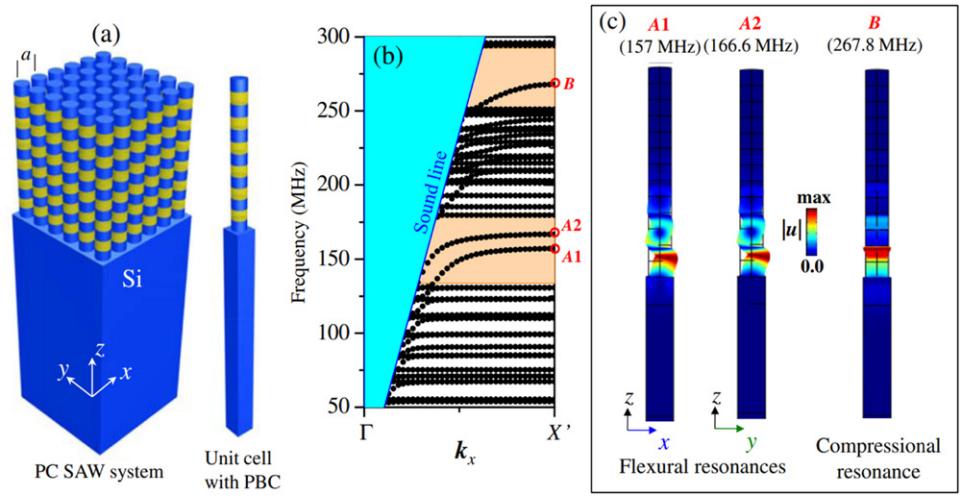

Fig. 22 (a) Structure of PnC consists of a square array of phononic pillars on Si substrate (b) wave dispersion plot subjected to SAW propagation along the *x* direction (c) total displacement field amplitude for modes A1, A2 and B. The figure is based on the result reported in Oudich *et al.* Reproduced from Oudich, M., Djafari-Rouhani, B., Bonello, B., *et al.*, 2018. Rayleigh waves in phononic crystal made of multilayered pillars: Confined modes, fano resonances, and acoustically induced transparency. Physical Review Applied 9 (3), 034013.

stacking behaves like a 1-D PnC that prohibits wave propagation along the vertical axis. Therefore, one can presume that such type of arrangement supports localized modes/defect state when subjected to incoming SAWs. The corresponding wave dispersion branch is presented in Fig. 22(b) along the $\Gamma - X$ direction of the Brillouin zone. The modes are confined at the surface of the silicon substrate and/or inside the pillars below the silicon sound line. However inside the BG region of periodic multilayer pillars, three distinct modes, designated as A1, A2 and B, emerge. On the other hand, the displacement fields of other SAW branches are distributed throughout the pillars. One can observe from Fig. 22(c), the vibration modes for these three modes are mainly localized at the bottom of the pillar that is close to interface of the pillar and substrate. Further, modes A1 and A2 are bending modes while mode B is likely longitudinal vibration.

Next, an array of pillars on the surface of semi-infinite Si substrate is considered that is subjected to incoming Rayleigh wave as shown in Fig. 23(a, b). The wave transmission response is presented in Fig. 23(c) that shows SAW attenuation inside the shaded (BG) region where drastic reduction in the displacement field amplitude $|u_z|$ at 161 MHz is observed. Further insight on the total displacement field plot, see Fig. 23(d), indicates that the Rayleigh wave attenuation is caused by interaction of incoming Rayleigh wave with A resonant mode of the 1-D periodic multilayer pillars.

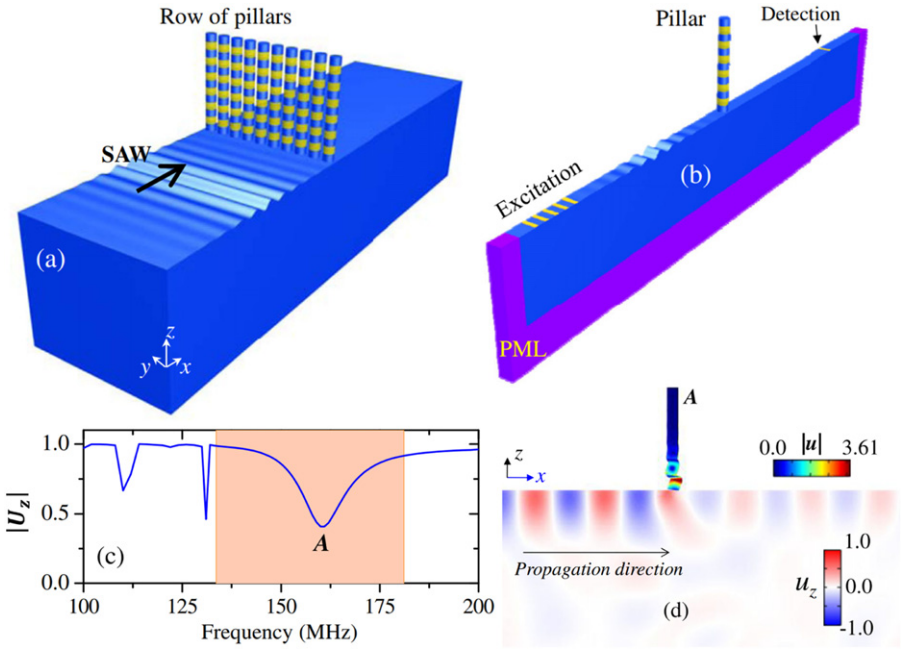

Fig. 23 (a) Schematic diagram for propagation of Rayleigh wave through a single row of PnC pillar (b) model adopted in FEM to calculate wave transmission, (c) wave transmission curve, (d) total displacement field in the pillar and Si substrate upon interaction with SAW. The figure is based on the result reported in Oudich *et al.* Reproduced from Oudich, M., Djafari-Rouhani, B., Bonello, B., *et al.*, 2018. Rayleigh waves in phononic crystal made of multilayered pillars: Confined modes, fano resonances, and acoustically induced transparency. Physical Review Applied 9 (3), 034013.

Low Frequency Bandgap Engineering

Trampoline Metamaterials

Since the fundamental work by Liu *et al.* (2000) on locally resonant sonic crystals governing low-frequency narrow local resonance BG, BG enlargement remains an unresolved problem. An enlarged low-frequency local resonance BG may find promising applications in low-frequency broadband wave control. Multiple approaches have been reported on PnC (Assouar and Oudich, 2012; Zhao *et al.*, 2015; Sigmund and Jensen, 2003; Bilal and Hussein, 2011) to help resolve this issue, however less attention is given to BG widening in locally resonant AMs. This section will put forward a brief insight on wave dispersion characteristics of AM that is formed by erection of pillars on the elastic plate covered by a periodic array of holes (Bilal and Hussein, 2013; Bilal *et al.*, 2017; Muhammad and Lim, 2020b). The term *trampoline effect* is intermittently used where the solid region of plate works as a springboard that reduces the plate stiffness and results in local resonance BG enlargement compare to pillar-plate structure with no holes. This so-called trampoline effect results in BG amplification at the subwavelength frequency regime. The aim of this section is to establish a brief insight on trampoline effect in the context of pillar-plate structure. A detailed study is reported by Bilal and Hussein (2013), Bilal *et al.* (2017) and later extended to multi-resonant structure (Muhammad and Lim, 2020b).

To understand the working mechanism for BG amplification caused by the trampoline effect, a general understanding for wave dispersion of homogenous plate and pillar-plate structure is necessary. The pillar and plate structure are crystalline silicon with material parameters stated in the prior sections. In **Fig. 24** (a-b), wave dispersion for homogenous plate with a periodic array of holes and solid pillar-plate structure is shown. The former does not possess any BG while the latter shows local resonance/hybridization BG. Next, a periodic array of holes is drilled inside the plate with diameter $d_h = 5a/8$, equivalent to pillar diameter. Introducing periodic array of holes inside the plate forges the plate to work as a springboard that intensifies the motion between pillar and remaining area of the plate confining the pillar. As a result the stiffness of plate reduces and we observe an amplification of the width of local resonance BG.

The idea of trampoline effect for hybridization BG amplification is fascinating where structural modification alters the dynamic characteristics of synthetic structures. However, the width of BG reported in **Fig. 24**(c) is narrow. One of the possible reasons is that both pillar and plate structures consist of same material. Recently, Muhammad *et al.* (2019a) proposed the idea of composite trampoline metamaterials for local resonance BG amplification. The evolution of composite trampoline metamaterials for basic pillar-plate structural block is shown in **Fig. 25**. In this approach, a solid pillar made of some soft materials like polymer is replaced by a hollow pillar and the hollow portion is filled with some stiffer materials like steel or aluminum. Such approach enhances the system effective mass density and this structural modification, when combined with the trampoline effect that is caused by drilling a periodic array of holes inside the plate, result in an enlarged local resonance BG at a subwavelength frequency regime.

The wave dispersion study for composite pillar and trampoline metamaterials is performed and band structures with BGs are depicted in **Fig. 26**. The introduction of steel cylinder inside the hollow polymeric pillar-plate structure enhances the effective mass

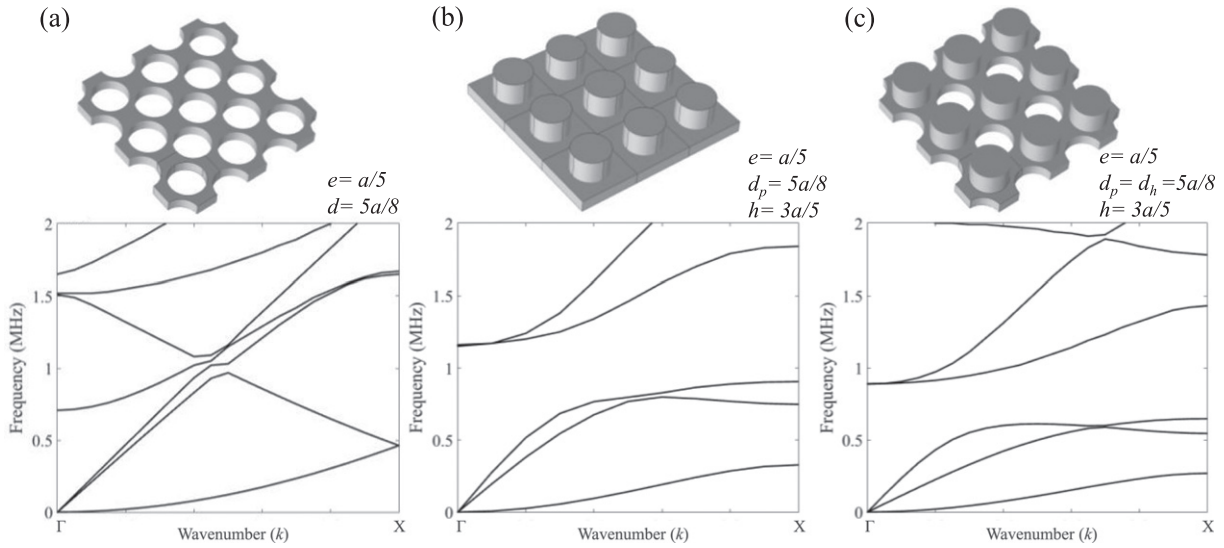

Fig. 24 Trampoline metamaterial demonstration. Top row shows schematic diagrams of (a) homogenous phononic plate structure with a periodic array of holes, (b) AM consists of a periodic array of pillars on the plate, and (c) trampoline metamaterial consisting of a periodic array of pillars deposited on plate having an array of identical holes. The widening of local resonance BG due to trampoline effect can be seen. The figure is based on the result reported in Bilal and Hussein Reproduced from Bilal, O.R., Hussein, M.I., 2013. Trampoline metamaterial: Local resonance enhancement by springboards. Applied Physics Letters 103 (11), 111901.

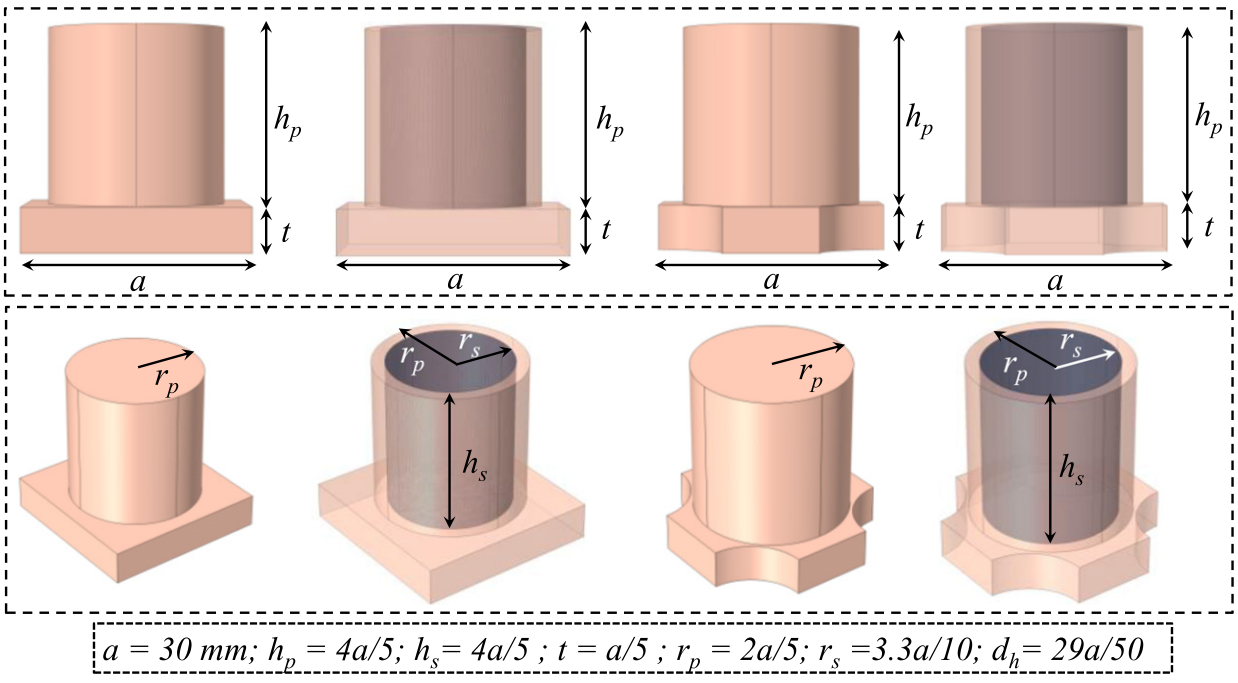

Fig. 25 Monolithic and composite pillar-plate structure (*top*) 2D and (*bottom*) 3D views. The polymeric and steel masses are differentiated by assigning creamy and black colors, respectively. All geometric parameters are presented at the inset of the figure. The figure is based on the result reported in Muhammad *et al.* Reproduced from Muhammad, Hussain, S.I., Lim, C.W., 2021a. Composite trampoline metamaterial with enlarged local resonance bandgap. Applied Acoustics 184.

density of the resonant system while the periodic array of holes reduces the plate stiffness. This cumulative effect results in an amplified local resonance BG with a relative bandwidth of about 100%. The finite pillar-plate structure based wave transmission study is presented aside the band structure. One can observe the attenuation of bulk elastic waves inside the BG frequency region.

Next, a parametric study is carried out to investigate the effect of steel inclusion height and diameter on the reported BGs, see Fig. 26. In Fig. 27 (a-d), it is shown that with increasing cylindrical steel height and diameter, the reported BG become wider and

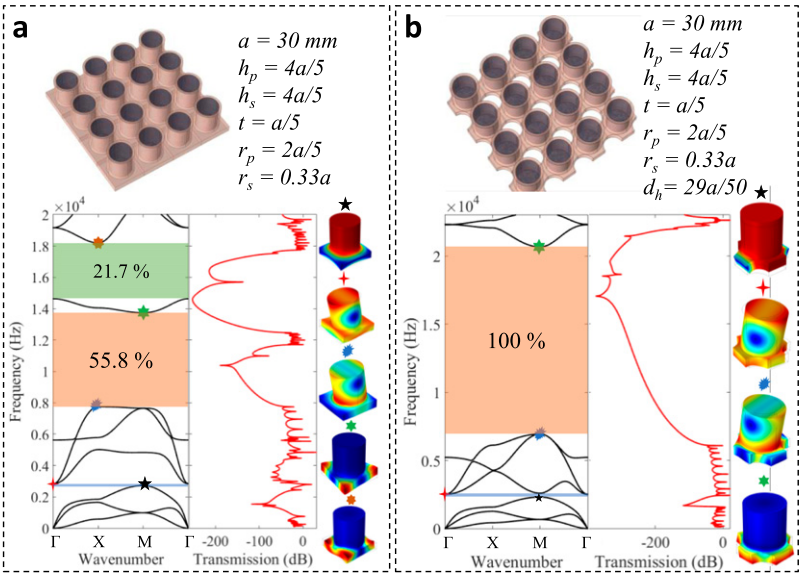

Fig. 26 Bulk band structure with frequency response spectra for composite pillar-plate structure and composite trampoline metamaterials. BGs are highlighted and relative bandwidth are presented at the inset. The bulk vibration modes responsible for opening and closing of BGs are presented on the right side of the frequency response spectrum. The figure is based on the result reported in Muhammad *et al.* Reproduced from Muhammad, Hussain, S.I., Lim, C.W., 2021a. Composite trampoline metamaterial with enlarged local resonance bandgap. Applied Acoustics 184.

the relative bandwidth increases. Conversely, a decrease in that geometric parameter leads to findings identical to monolithic pillar-plate structure as explained in the prior sections. Therefore, converting a monolithic pillar with composite one and combining with trampoline effect actually increases the BG width and shift the frequency region to a subwavelength regime. Further details are given in Muhammad *et al.* (2021a).

Tailored Elastic Metamaterials

The idea of trampoline effect in AM for hybridization BG enlargement is discussed in the previous section. This section will put forward an insight on another governing mechanism that helps widen Bragg BG and extend BG to a low-frequency region. The physical model for pillar-plate structure is identical to that discussed in Section "Hollow Phononic Pillars Subjected to Lamb Waves". Here, the pillars are connected to each other with the help of cross bar instead of plate as the base medium. The width of bar is $b/a = 0.1,\ 0.5,\ 1$ see **Fig. 28**. Before putting a detailed insight on the governing Bragg BG enlargement mechanism, the band structure of pillar structure with cross bar $b/a = 1$ is analyzed first. As shown in **Fig. 28**(a), Bragg and local resonance BGs appear along the $\Gamma - X$ direction of the Brillouin zone. Now a tailored metamaterial that consists of tunable crossing of two bars is proposed as shown in **Fig. 28**(b). When the width of bar is reduced by a half i.e., $b/a = 0.5$, the four corners of unit cell structure is converted to eight corners. This structural modification alters the wave dispersion and it results in further widening of Bragg BG, see **Fig. 28**(b). Likewise, for $b/a = 0.1$ a further widening of Bragg BG is observed as highlighted. It is also observed that BG shifts towards a low frequency regime. The reduction in b/a also shifts the hybridization gap toward a lower frequency region. For more details, one can refer to Jin *et al.* (2016c).

Rainbow Metamaterials

The disorder in rainbow metamaterials is another effective approach recently reported for widening local resonance BG. The idea is initially reported by Tsakmakidis *et al.* (2007) for rainbow trapping of light wave, i.e., to trap and store light wave energy. Later, Zhu *et al.* (2013) extended the idea to acoustic rainbow effect where acoustic wave trapping and separation over broadband frequency region is demonstrated both theoretically and experimentally by graded arrangement of resonators. Likewise, recently Meng *et al.* (2020) applied similar approach for broadband multi-frequency vibration control through numerical and experimental means. The idea of disorder rainbow metamaterials for BG widening and elastic wave manipulation is recently proposed by Celli *et al.* (2019). A metamaterial setup in the form of a stubbed plate (a pillar like resonator deposited on a thin elastic sheet) can display subwavelength local resonance BG. The frequency BG region can be widened by introducing graded arrangements of resonators where the spatial distribution of resonance frequency leads to broadband BG that covers a large frequency spectrum. Recently, Celli *et al.* (2019) envisaged widening of local resonance BG caused by disorder/random arrangements of pillar like resonators on a thin elastic sheet. Both spatially graded and disordered arrangements of stubbed plates resulted in further widening of BG. However, BG widening caused by heterogeneously tuned resonators is greater than the homogenous and graded counterpart. This is because a plate structure that is significantly compliant with respect to pillar resonators, transmission of elastic waves across the structure becomes dependent

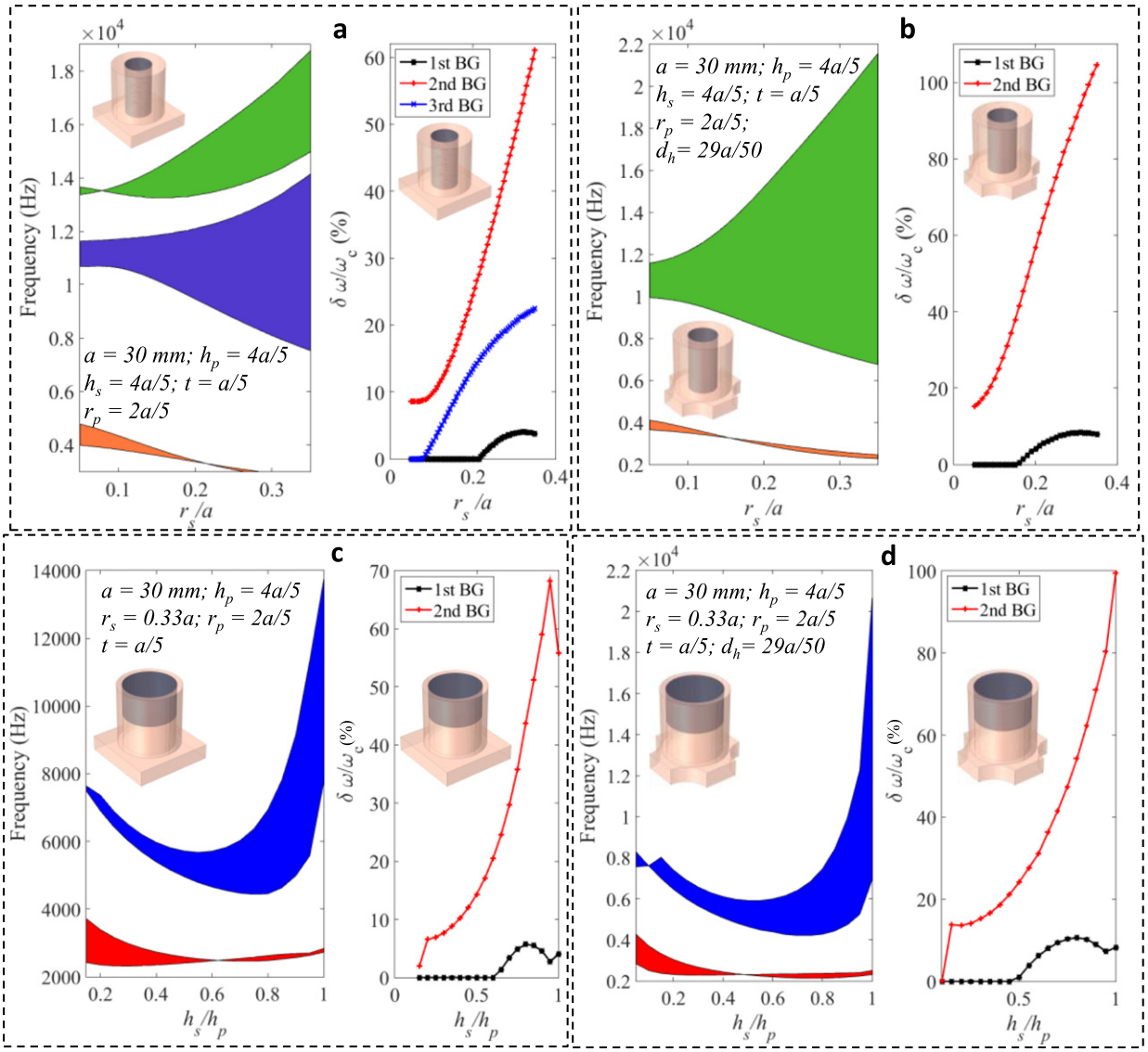

Fig. 27 Effect of cylindrical inclusion geometric parameters on the reported BGs. The relative bandwidth is also shown aside. The figure is based on the result reported in Muhammad *et al.* Reproduced from Muhammad, Hussain, S.I., Lim, C.W., 2021a. Composite trampoline metamaterial with enlarged local resonance bandgap. Applied Acoustics 184.

on the spatial arrangements of resonators. Such effect can be seen in **Fig. 29** where homogenous, graded and random arrangement of pillar resonators is compared. One can observe further widening of local resonance BG caused by disorder arrangement of pillar resonators. Subsequent to Celli *et al.* (2019), Muhammad *et al.* (2021c) numerically showed such effect for disordered arrangement of forest trees subjected to surface Rayleigh wave. Therefore, it is substantiated that even heterogenous arrangement of pillars/resonators that are distinct from each other in term of spatial characteristics result in wider BG as compared to homogenous or graded counterparts. Further details can be found in Celli *et al.* (2019).

Topological Protected Phononic Pillared Structures

Introduction

Recently a surge of research studies has been reported for mechanical analogs of topologically protected edge modes including analogies with the quantum hall effect, quantum spin hall effect, valley hall effect, etc. These studies are fundamentally linked to some pioneering works (Klitzing *et al.*, 1980; Tsui *et al.*, 1982; Haldane, 1983) that pave the way for a newly emerging field of topological physics and mechanics with wave energy localization and insulation characteristics. For early treatment of topological systems in elastic media one can refer to Wang *et al.* (2015). For a detailed discussion on topological principles to acoustic and

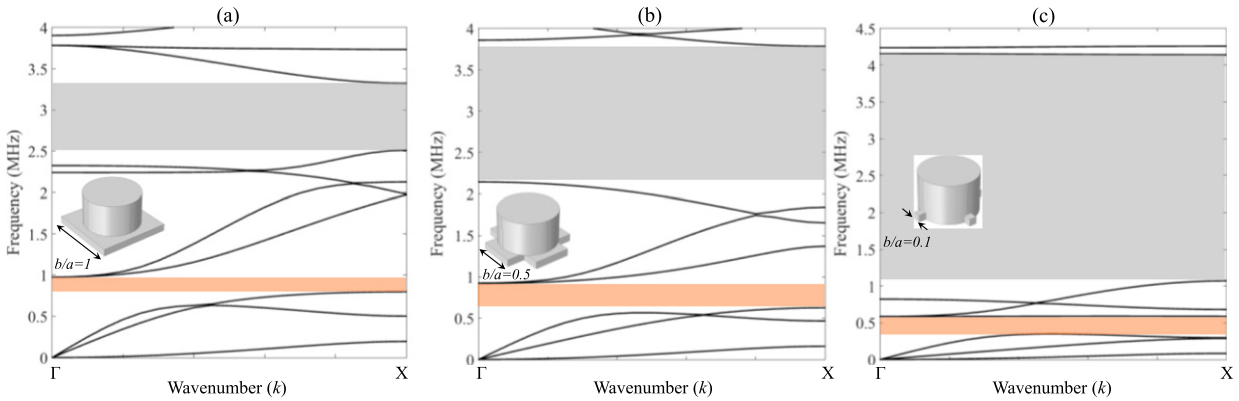

Fig. 28 Wave dispersion study for tailored elastic metamaterials. The phononic pillar is connected with two thin bars of width b/a. The local resonance and Bragg BGs are highlighted. (a) Band structure for simple pillar-plate structure with $b/a = 1$, (b) $b/a = 0.5$ (c) $b/a = 0.1$ in the $\Gamma - X$ direction of the Brillouin zone. The figure is based on the result reported in Jin *et al.* Reproduced from Jin, Y., Pennec, Y., Pan, Y., *et al.*, 2016c. Phononic crystal plate with hollow pillars connected by thin bars. Journal of Physics D: Applied Physics 50 (3), 035301.

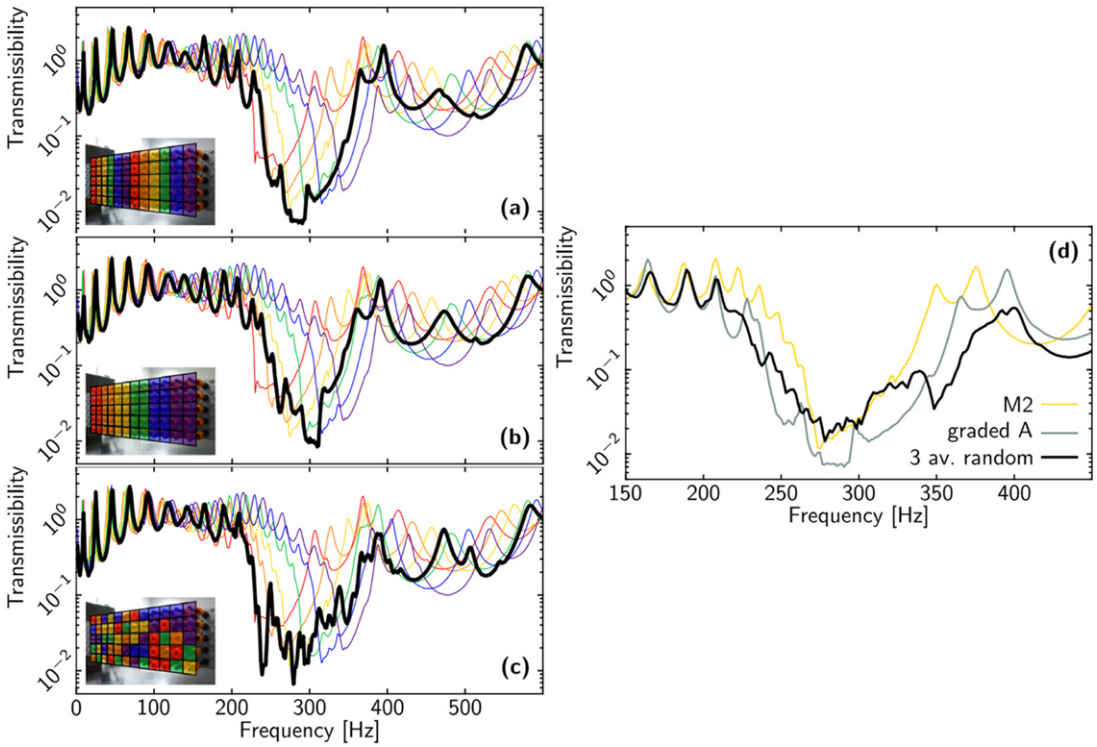

Fig. 29 Disorder rainbow metamaterials: Influence of spatial distribution of pillar resonators on wave transmission and attenuation. In total six types of arrangements are considered and transmissibility values are compared. Transmissibility for graded configuration is depicted as (a) group A, (b) group B, (c) spatially disorder arrangement, and (d) BG comparison for different arrangements. The figure is based on the result reported in Celli *et al.* Reproduced from Celli, P., Yousefzadeh, B., Daraio, C., *et al.*, 2019. Bandgap widening by disorder in rainbow metamaterials. Applied Physics Letters 114 (9), 091903.

elastic media one can refer to some recent reviews (Zhang *et al.*, 2018; Ma *et al.*, 2019; Muhammad and Lim, 2021a). Among other enriched wave dispersion characteristics, phononic pillared plate structure also exhibits topological edge states and interface modes with wave energy localization that is immuned to backscattering effects. By classifying the pillar as a point-like resonator coupled to the plate by a spring for out-of-plane vibrations, an analytical theory for a pillared phononic plate in terms of flexural waves was devised Xiao *et al.* (2012). Similarly, Torrent *et al.* (2013) presented Dirac cones due to lattice symmetry as a counterpart of graphene. Further, analytical equations of Dirac frequency and velocity for honeycomb lattice are derived. By breaking the time reversal symmetry or inversion symmetry in the honeycomb lattice, band degeneracy at Dirac point and opening of BG caused by

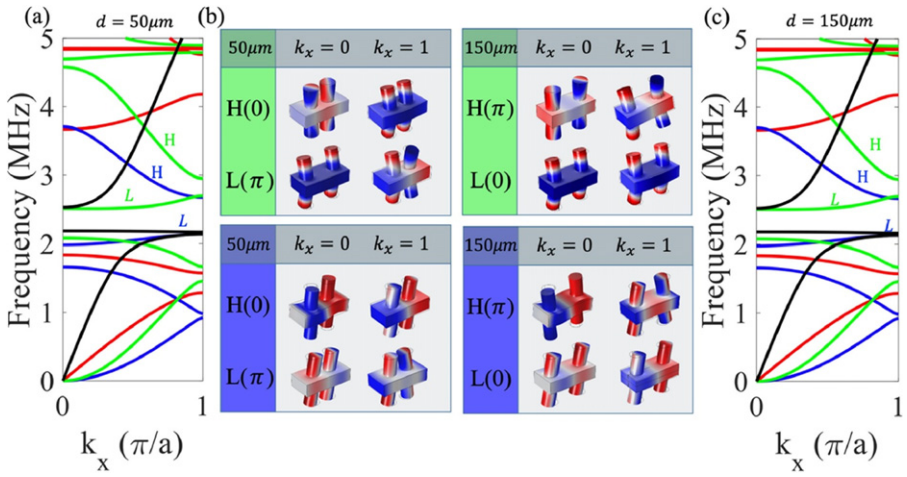

Fig. 30 Dirac cone band degeneracy and opening of BG caused by lifting of degeneracy point. (a, c) Band structure, (c) geometric phases at the center and edge of the Brillouin zone. The figure is based on the result reported in Jin *et al.* Reproduced from Jin, Y., Wang, W., Djafari-Rouhani, B., 2020a. Asymmetric topological state in an elastic beam based on symmetry principle. International Journal of Mechanical Sciences 186, 105897.

lifting of Dirac point is observed. It was demonstrated that the topological invariant bands have nonzero Chern number that affirm the nontrivial topological property allowing the governance of topologically protected interface states at the interface of topological distinct crystals. Likewise, some recent studies (Wang *et al.*, 2020; Jin *et al.*, 2020a) demonstrated that topological Fano resonance can also be induced through combining both topological dark and bright modes in a pillared beam setup. One such example is shown in **Fig. 30** where geometric phase transition can be observed.

Topologically Protected States

Before delving into topologically protected states/edge modes, an understanding of topological mechanics and its relationship with quantum mechanics alongside topological insulators is necessary. Topological insulators are electronic materials with bulk BG identical to the common insulators. They possess conducting states on the surface and/or edges. Such property cannot be observed in naturally occurring materials and their peculiar behavior is accredited to the time reversal symmetry and spin-orbital interaction of atoms and electrons. Now when one talks about topology, it describes the global properties of wavefunction in a band structure and it pertains to the robust behavior against local perturbation, therefore maintaining certain symmetric properties unless the perturbation is sufficiently strong enough to close the BGs through symmetry breaking (Ma *et al.*, 2019). Underneath these principles and some others (Yang *et al.*, 2015; Zhang *et al.*, 2018; Ma *et al.*, 2019), the field of topological physics and mechanics has found a strong route in artificial periodic structures like PnCs and AMs. A fantastic property of interest is the presence of topologically protected edge modes/states at the interface of topologically distinct structures with robust wave energy localization, immune to backscattering, and deflection to sharp edges and corners (Xiao *et al.*, 2015; Miniaci *et al.*, 2018; Muhammad and Lim, 2020a; Muhammad *et al.*, 2021b). In the context of a pillared plate model focused in this article, there exist multiple studies that explore topological properties with edge modes. Here we summarize some of the works reported in that context.

By establishing an analytical model of pillar-like point resonators on a homogenous plate and breaking the inversion symmetry, (Pal and Ruzzene, 2017) established topologically protected edges states. Later, the findings were further confirmed by experiment reported by Vila *et al.* (2017). For equal pillar masses, the double sided hexagonal lattice depicts a Dirac cone at the K/K′ points in the Brillouin zone. By breaking the mirror symmetry of a unit cell structure via introduction of different masses (varying geometric parameters of the pillar) see **Fig. 31**, a Dirac cone degeneracy point can be lifted and nontrivial BG can be envisaged. Analyzing the valley Chern number for these eigenmodes indicate opposite polarization i.e., ½ and -½ that illustrate the analogy with quantum valley hall effect. By building the finite strip of a unit cell structure, interface mode frequency with robust wave energy localization can be observed at the interface of topologically distinct pillar masses. Also, if one performs wave dispersion study for finite strip, an interface band in the bulk nontrivial BG with localized eigenmode as topologically protected edge state can be seen.

Similarly, Chaunsali *et al.* (2018) proposed a topological hexagonal lattice where the six bolt-like pillars are arranged in such a manner to make it easily shrinkable and expandable. The pseudospin Hall effect for flexural wave with local resonators was demonstrated. The formation and degeneracy of a double Dirac cone at the K/K′ symmetry points are presented and opening of a Bragg BG is depicted that is caused by variation in translational periodicity. By combing the trivial and nontrivial edge mode lattices, the interface states are presented. Likewise, recently Jin *et al.* (2020b) studied topological states in a twisted pillared phononic plate structure with interface modes and wave energy localization. In another work Jin *et al.* (2018) investigated the effect of defect in a supercell hexagonal lattice structure on protected interface mode. It is deduced that with the presence of defect, the immunity to backscattering and lossless wave energy propagation across sharp edges prevail and the finding suggest that compare to a defect state, energy localization at interface mode frequency is quite robust, as shown in

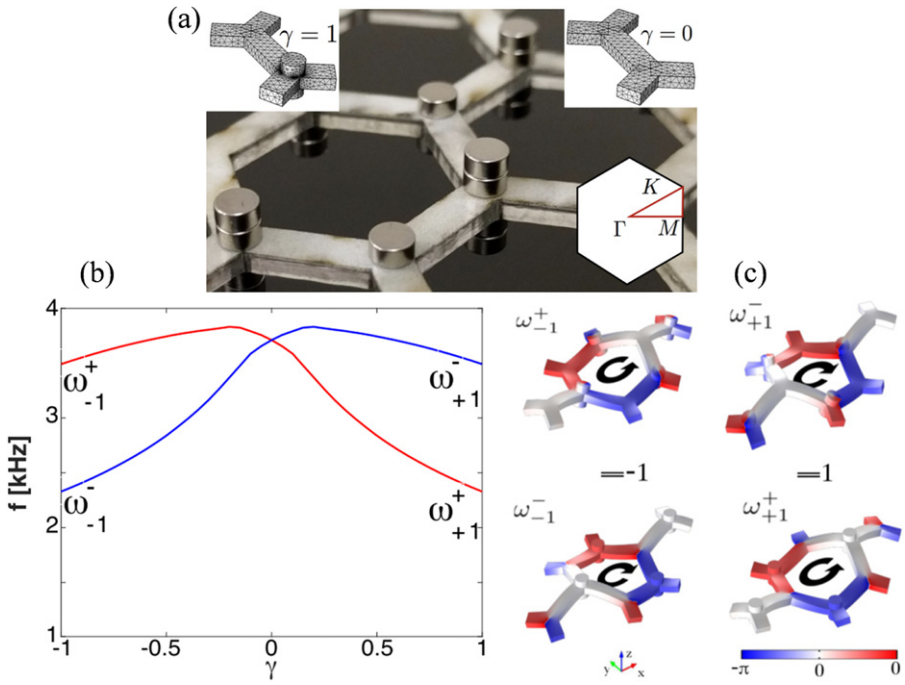

Fig. 31 (a) Experimental lattice with added pillared masses at the sublattice sites. At the inset, FE discretization of a unit cell structure with $\gamma = 1$ and $\gamma = 0$ for numerical study is depicted. The first irreducible Brillouin zone is shown at the inset. (b) Band inversion at the bounding BG edges, (c) geometric phases of the initial two eigenfrequencies with out-of-plane mode polarization at *K* point for $\gamma = -1$ and $\gamma = 1$. The figure is based on the result reported in Vila *et al.* Reproduced from Vila, J., Pal, R.K., Ruzzene, M., 2017. Observation of topological valley modes in an elastic hexagonal lattice. Physical Review B 96 (13), 134307.

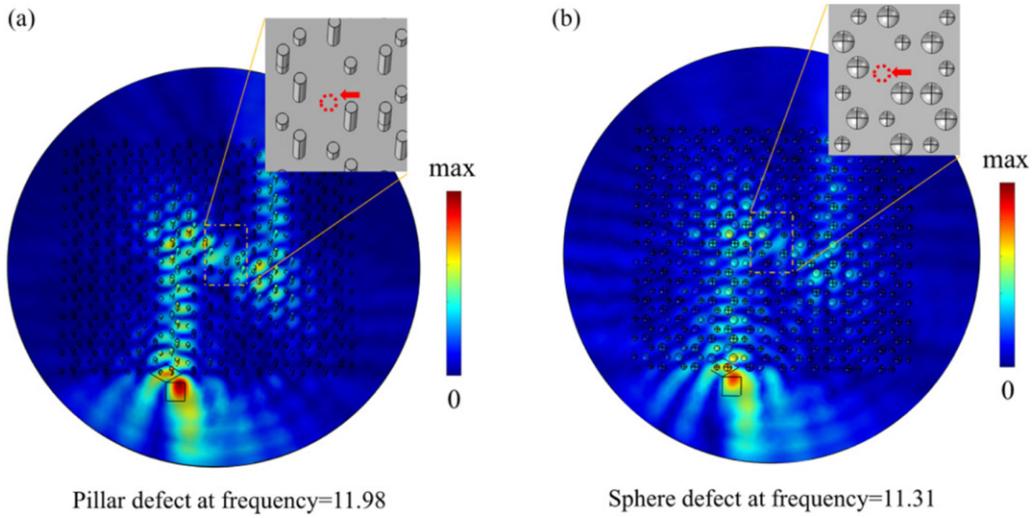

Fig. 32 Excitation topological edge state at reduced frequency, (a) 11.98 for pillar scatter, and (b) 11.31 for the sphere scatter with the presence of defect. The defect state is induced by removing one sphere/cylinder. The amplitude of out-of-plane displacement u_z is shown by color bars. The figure is based on the result reported in Jin *et al.* Reproduced from Jin, Y., Torrent, D., Djafari-Rouhani, B., 2018. Robustness of conventional and topologically protected edge states in phononic crystal plates. Physical Review B 98 (5), 054307.

Fig. 32(a). Even though a defect is planted on the substrate, robust propagation of wave energy along a zig-zag path can be observed. However, if local perturbation is not strong enough to open the nontrivial BG and the edge band is disturbed, the robustness of protected edge states will diminishes and fail to preserve edge propagations. This can be monitored from Fig. 32 (b) where the size of bulk structure surrounding the zig-zag interface is minimized. Although the shape of zigzag interface propagation is preserved, the surrounding bulk media for sharp edge show the presence of minimized wave energy.

Conclusion and Future Outlook

The main objective of this article is to establish a deep insight on different characteristics of pillared phononic materials and their vibration resonance properties. Since the initial studies in 2008, pillared based phononic structures have been widely investigated as phononic crystals, acoustic/elastic metamaterials, metasurfaces and topological structures for acoustic and elastic waves manipulation. By tailoring the local resonance and Bragg scattering properties of the branching pillars, numerous avenues for acoustic and elastic waves manipulation have been explored. This articulative structures still inspire fundamentally new phenomena both in wave physics and solid mechanics today. This book article begins with a detailed overview on phononic crystals and metamaterials with an insight on the physical concepts and mechanical background. Both indispensable topics are distinguished by discussing the fundamental properties that may help readers to differentiate the ideas. The discussion on fundamental concepts in these artificial structures are followed by a historical context and recent developments in the field of pillared phononic crystals and metamaterials. An insight on possible potential applications is also presented. Furthermore, Bragg BG and low-frequency local resonance/hybridization gap exhibition by pillared structure and their tunability for waveguiding applications are explored. These fundamental principles are explained for symmetric and antisymmetric Lamb waves and surface acoustic waves separately. In the perspective of waveguiding, the localized cavity mode of phononic pillars, the so-called whispering gallery modes subject to Lamb waves and SAWs are discussed. Likewise, manipulation of Lamb waves and SAWs by multilayer phononic pillars and their resonance phenomena are also explained and peculiar wave effects are depicted. A brief discussion on trampoline effect and tailored acoustic metamaterials is also covered. These are two dominant mechanisms reported to enlarge hybridization and Bragg BGs, respectively. In addition, the recently reported idea of disorder rainbow metamaterials, that is based on a stubbed plate model for widening the local resonance BG, is also explained. Pillared structures also exhibit rich physical properties in the field of topological physics and mechanics. Such structures when arranged appropriately exhibit topologically protected interface states with robust wave localization and propagation along a designated path(s). We discuss some recent developments in the field and refer to updated literature for more details. In general this article puts forward an effort to explore the peculiar dynamics characteristics of pillared phononic structures in the context of phononic crystals and metamaterials. The works covered and references highlighted may help the readers to grasp the fundamental concepts in this field in the hope of widening their horizon in search of new avenues to overcome future challenges and pave the way to real-life engineering applications.

Although the field of phononic crystals and metamaterials in general and pillared structures in particular has seen tremendous research growth in the past two decades, there remains plenty of rooms for further advancements and improvements. Some of the challenges involved are highlighted below that could most probably be overcome in the near future.

- A number of fascinating works have covered pillared resonance with different orders by considering classical mechanics theories and numerical modeling approaches (Torrent *et al.*, 2013; Chaunsali *et al.*, 2018). There still exist some needs for a rigorous mathematical modeling based on homogenization theory and numerical modeling like the multiple scattering method or wavelet based method for analyzing the in-plane displacement of pillar modes in 3D continuous elastic models.
- Currently phononic materials and metamaterials research works are more oriented towards periodic arrangement of structures, pillared structures in the context of this article. Less attention has been devoted to the dynamically reached random arrangements of resonators. Such investigations may pave the way for novel physical phenomena and wave effects that have not been observed in these structures. This is possible as the key dynamic properties of metamaterials do not depend upon system periodicity.
- Multiple studies have explored waveguiding, defect and focusing effects by pillared structures. Topological properties by pillared structures subject to Lamb waves and surface acoustic waves have not been analyzed in detail. Although there are some works on topologically protected interface modes in pillared structures subject to out-of-plane A_0 Lamb wave, the presence of such interface mode for in-plane wave and surface acoustic wave is yet to be explored both in theory and experiment. We expect new findings in this respect by pillared phononic structures to be reported in the near future.
- Apart from the dual Bragg and hybridization gaps properties, pillared *PhoXonic crystal* is another potential research avenue that provides a common platform to manipulate both photons (electromagnetic and light waves) and phonons (acoustic and elastic waves). Although some works have numerically proven this concept (Rolland *et al.*, 2012), a rigorous mathematical model with experimental works may result in new discoveries in this newly emerging field.
- Optimization of pillared structures by data-driven machine learning and deep learning methods is an unexplored research subject. Recently, these data-driven tools have seen tremendous research interest in the field of phononic crystals and metamaterials with some promising results (Kollmann *et al.*, 2020; Li *et al.*, 2020; Gurbuz *et al.*, 2021). Most optimization works on pillared structures are based on human-intuitive design approaches. A general parametric study on the topology optimization method that is not data-driven and that works without preconceived shape information is very desirable. Machine learning and deep learning methods may enrich the dynamical properties of pillared structures and make the wave dispersion and finite length modeling approaches independent of numerical simulations.

References

Achaoui, Y., Khelif, A., Benchabane, S., *et al.*, 2011. Experimental observation of locally-resonant and Bragg band gaps for surface guided waves in a phononic crystal of pillars. Physical Review B 83 (10), 1–5.

Addouche, M., Al-Lethawe, M.A., Choujaa, A., *et al.*, 2014. Superlensing effect for surface acoustic waves in a pillar-based phononic crystal with negative refractive index. Applied Physics Letters 105 (2), 023501.

Al-Lethawe, M.A., Addouche, M., Khelif, A., *et al*., 2012. All-angle negative refraction for surface acoustic waves in pillar-based two-dimensional phononic structures. New Journal of Physics 14 (12), 123030.
Alu, A., Silveirinha, M.G., Salandrino, A., *et al*., 2007. Epsilon-near-zero metamaterials and electromagnetic sources: Tailoring the radiation phase pattern. Physical Review B 75 (15), 155410.
Assouar, B., Oudich, M., Zhou, X., 2016. Acoustic metamaterials for sound mitigation. Comptes Rendus Physique 17 (5), 524–532.
Assouar, B., Liang, B., Wu, Y., *et al*., 2018. Acoustic metasurfaces. Nature Reviews Materials 3 (12), 460–472.
Assouar, M.B., Oudich, M., 2012. Enlargement of a locally resonant sonic band gap by using double-sides stubbed phononic plates. Applied Physics Letters 100 (12), 123506.
Badreddine Assouar, M., Sun, J.-H., Lin, F.-S., *et al*., 2014. Hybrid phononic crystal plates for lowering and widening acoustic band gaps. Ultrasonics 54 (8), 2159–2164.
Banerjee, A., Das, R., Calius, E.P., 2018. Waves in structured mediums or metamaterials: A review. Archives of Computational Methods in Engineering 26 (4), 1029–1058.
Bilal, O.R., Hussein, M.I., 2011. Ultrawide phononic band gap for combined in-plane and out-of-plane waves. Physical Review E: Statistical, Nonlinear, and Soft Matter Physics 84 (6 Pt 2), 065701.
Bilal, O.R., Hussein, M.I., 2013. Trampoline metamaterial: Local resonance enhancement by springboards. Applied Physics Letters 103 (11), 111901.
Bilal, O.R., Foehr, A., Daraio, C., 2017. Observation of trampoline phenomena in 3D-printed metamaterial plates. Extreme Mechanics Letters 15, 103–107.
Carrara, M., Cacan, M.R., Toussaint, J., *et al*., 2013. Metamaterial-inspired structures and concepts for elastoacoustic wave energy harvesting. Smart Materials and Structures 22 (6), 065004.
Celli, P., Yousefzadeh, B., Daraio, C., *et al*., 2019. Bandgap widening by disorder in rainbow metamaterials. Applied Physics Letters 114 (9), 091903.
Chaplain, G.J., De Ponti, J.M., Colombi, A., *et al*., 2020. Tailored elastic surface to body wave Umklapp conversion. Nature Communications 11 (1), 3267.
Chaunsali, R., Chen, C.-W., Yang, J., 2018. Subwavelength and directional control of flexural waves in zone-folding induced topological plates. Physical Review B 97 (5), 054307.
Chen, H., Chan, C.T., Sheng, P., 2010. Transformation optics and metamaterials. Nature Materials 9 (5), 387–396.
Colombi, A., 2016. Resonant metalenses for flexural waves in plates. The Journal of the Acoustical Society of America 140 (5), EL423–EL428.
Colombi, A., Colquitt, D., Roux, P., *et al*., 2016a. A seismic metamaterial: The resonant metawedge. Scientific Reports 6.27717.
Colombi, A., Roux, P., Guenneau, S., *et al*., 2016b. Forests as a natural seismic metamaterial: Rayleigh wave bandgaps induced by local resonances. Scientific Reports 6.19238.
Colquitt, D.J., Colombi, A., Craster, R.V., *et al*., 2017. Seismic metasurfaces: Sub-wavelength resonators and Rayleigh wave interaction. Journal of the Mechanics and Physics of Solids 99, 379–393.
Davis, B.L., Hussein, M.I., 2014. Nanophononic metamaterial: Thermal conductivity reduction by local resonance. Physical Review Letters 112 (5), 055505.
De Ponti, J.M., Colombi, A., Ardito, R., *et al*., 2020. Graded elastic metasurface for enhanced energy harvesting. New Journal of Physics 22 (1), 013013.
DePauw, D., Al Ba'ba'a, H., Nouh, M., 2018. Metadamping and energy dissipation enhancement via hybrid phononic resonators. Extreme Mechanics Letters 18, 36–44.
Djafari Rouhani, B., Pennec, Y., El Boudouti, E.H., *et al*., 2011. Band gap engineering in simultaneous phononic and photonic crystal slabs. Applied Physics A 103 (3), 735–739.
Djafari-Rouhani, B., Pennec, Y., Larabi, H., 2010. Band structure and phonon transport in a phononic crystal made of a periodic array of dots on a membrane. In: Wu, T.-T., Ma, C.-C. (Eds.), IUTAM Symposium on Recent Advances of Acoustic Waves in Solids. Springer, pp. 127–138.
El Hassouani, Y., Li, C., Pennec, Y., *et al*., 2010. Dual phononic and photonic band gaps in a periodic array of pillars deposited on a thin plate. Physical Review B 82 (15), 155405.
Foreman, M.R., Swaim, J.D., Vollmer, F., 2015. Whispering gallery mode sensors. Advances in Optics and Photonics 7 (2), 168–240.
Graczykowski, B., Mielcarek, S., Trzaskowska, A., *et al*., 2012. Tuning of a hypersonic surface phononic band gap using a nanoscale two-dimensional lattice of pillars. Physical Review B 86 (8), 085426.
Guo, Y., Hettich, M., Dekorsy, T., 2017. Guiding of elastic waves in a two-dimensional graded phononic crystal plate. New Journal of Physics 19 (1), 013029.
Gurbuz, C., Kronowetter, F., Dietz, C., *et al*., 2021. Generative adversarial networks for the design of acoustic metamaterials. The Journal of the Acoustical Society of America 149 (2), 1162–1174.
Haldane, F.D.M., 1983. Fractional quantization of the hall effect: A hierarchy of incompressible quantum fluid states. Physical Review Letters 51 (7), 605–608.
Huang, H.H., Sun, C.T., Huang, G.L., 2009. On the negative effective mass density in acoustic metamaterials. International Journal of Engineering Science 47 (4), 610–617.
Hussein, M.I., El-Kady, I., 2011. Preface to special topic: Selected articles from phononics 2011: The first international conference on phononic crystals, metamaterials and optomechanics. AIP Advances 1.
Hussein, M.I., Leamy, M.J., Ruzzene, M., 2014. Dynamics of phononic materials and structures: historical origins, recent progress, and future outlook. Applied Mechanics Reviews 66 (4), 040802.
Hussein, M.I., Tsai, C.-N., Honarvar, H., 2020. Thermal conductivity reduction in a nanophononic metamaterial versus a nanophononic crystal: A review and comparative analysis. Advanced Functional Materials 30 (8), 1906718.
Jin, Y., Fernez, N., Pennec, Y., *et al*., 2016a. Tunable waveguide and cavity in a phononic crystal plate by controlling whispering-gallery modes in hollow pillars. Physical Review B 93 (5), 054109.
Jin, Y., Pennec, Y., Pan, Y., *et al*., 2016b. Phononic crystal plate with hollow pillars actively controlled by fluid filling. Crystals 6 (6),
Jin, Y., Pennec, Y., Pan, Y., *et al*., 2016c. Phononic crystal plate with hollow pillars connected by thin bars. Journal of Physics D: Applied Physics 50 (3), 035301.
Jin, Y., Ei Boudouti, E.I.H., Pennec, Y., *et al*., 2017. Tunable Fano resonances of Lamb modes in a pillared metasurface. Journal of Physics D Applied Physics 50 (42), 425304.
Jin, Y., Torrent, D., Djafari-Rouhani, B., 2018. Robustness of conventional and topologically protected edge states in phononic crystal plates. Physical Review B 98 (5), 054307.
Jin, Y., Wang, W., Djafari-Rouhani, B., 2020a. Asymmetric topological state in an elastic beam based on symmetry principle. International Journal of Mechanical Sciences 186.105897.
Jin, Y., Wang, W., Wen, Z., *et al*., 2020b. Topological states in twisted pillared phononic plates. Extreme Mechanics Letters 39.100777.
John, S., 1987. Strong localization of photons in certain disordered dielectric superlattices. Physical Review Letters 58 (23), 2486–2489.
Kafesaki, M., Economou, E.N., 1999. Multiple-scattering theory for three-dimensional periodic acoustic composites. Physical Review B 60 (17), 11993–12001.
Khelif, A., Achaoui, Y., Aoubiza, B., 2012. Surface acoustic waves in pillars-based two-dimensional phononic structures with different lattice symmetries. Journal of Applied Physics 112 (3), 033511.
Klitzing, Kv, Dorda, G., Pepper, M., 1980. New method for high-accuracy determination of the fine-structure constant based on quantized hall resistance. Physical Review Letters 45 (6), 494–497.
Kollmann, H.T., Abueidda, D.W., Koric, S., *et al*., 2020. Deep learning for topology optimization of 2D metamaterials. Materials & Design 196.109098.
Koschny, T., Kafesaki, M., Economou, E.N., *et al*., 2004. Effective medium theory of left-handed materials. Physical Review Letters 93 (10), 107402.
Kushwaha, M.S., Halevi, P., Martinez, G., *et al*., 1994. Theory of acoustic band structure of periodic elastic composites. Physical Review B: Condensed Matter 49 (4), 2313–2322.
Li, F., Xuan, M., Wu, Y., *et al*., 2013. Acoustic whispering gallery mode coupling with Lamb waves in liquid. Sensors and Actuators A: Physical 189, 335–338.
Li, X., Ning, S., Liu, Z., *et al*., 2020. Designing phononic crystal with anticipated band gap through a deep learning based data-driven method. Computer Methods in Applied Mechanics and Engineering 361.112737.
Li, Y., Chen, T., Wang, X., *et al*., 2015. Enlargement of locally resonant sonic band gap by using composite plate-type acoustic metamaterial. Physics Letters A 379 (5), 412–416.
Li, Y., Zhu, L., Chen, T., 2017. Plate-type elastic metamaterials for low-frequency broadband elastic wave attenuation. Ultrasonics 73, 34–42.
Liu, Z., Zhang, X., Mao, Y., *et al*., 2000. Locally resonant sonic materials. Science 289 (5485), 1734–1736.
Ma, G., Xiao, M., Chan, C.T., 2019. Topological phases in acoustic and mechanical systems. Nature Reviews Physics 1 (4), 281–294.
Meng, H., Chronopoulos, D., Fabro, A.T., *et al*., 2020. Rainbow metamaterials for broadband multi-frequency vibration attenuation: Numerical analysis and experimental validation. Journal of Sound and Vibration 465.115005.
Miniaci, M., Pal, R.K., Morvan, B., *et al*., 2018. Experimental observation of topologically protected helical edge modes in patterned elastic plates. Physical Review X 8 (3).

Muhammad, Lim, C.W., 2020a. Analytical modeling and computational analysis on topological properties of 1-D phononic crystals in elastic media. Journal of Mechanics of Materials and Structures 15 (1), 15–35.
Muhammad, Lim, C.W., 2020b. Dissipative multiresonant pillared and trampoline metamaterials with amplified local resonance bandgaps and broadband vibration attenuation. Journal of Vibration and Acoustics 142 (6), 061012.
Muhammad, Lim, C.W., 2021a. From photonic crystals to seismic metamaterials: A review via phononic crystals and acoustic metamaterials. Archives of Computational Methods in Engineering 29.https://doi.org/10.1007/s11831-021-09612-8.
Muhammad, Lim, C.W., 2021b. Natural seismic metamaterials: The role of tree branches in the birth of Rayleigh waves bandgap. Trees 1.
Muhammad, Lim, C.W., 2021c. Phononic metastructures with ultrawide low frequency three-dimensional bandgaps as broadband low frequency filter. Scientific Reports 11 (1), 7137.
Muhammad, Lim, C.W., 2021d. Ultrawide bandgap by 3D monolithic mechanical metastructure for vibration and noise control. Archives of Civil and Mechanical Engineering 21 (2), 52.
Muhammad, Lim, C.W., Reddy, J.N., 2019a. Built-up structural steel sections as seismic metamaterials for surface wave attenuation with low frequency wide bandgap in layered soil medium. Engineering Structures 188, 440–451.
Muhammad, Zhou, W., Lim, C.W., 2019b. Topological edge modeling and localization of protected interface modes in 1D phononic crystals for longitudinal and bending elastic waves. International Journal of Mechanical Sciences 159, 359–372.
Muhammad, Lim, C.W., Reddy, J.N., *et al.*, 2020. Surface elastic waves whispering gallery modes based subwavelength tunable waveguide and cavity modes of the phononic crystals. Mechanics of Advanced Materials and Structures 27 (13), 1053–1064.
Muhammad, Hussain, S.I., Lim, C.W., 2021a. Composite trampoline metamaterial with enlarged local resonance bandgap. Applied Acoustics 184.
Muhammad, Lim, C.W., Leung, A.Y.T., 2021b. Plane and surface acoustic waves manipulation by three-dimensional composite phononic pillars with 3D bandgap and defect Analysis. Acoustics 3 (1), 25–41.
Muhammad, Wu, T., Lim, C.W., 2021c. Forest trees as naturally available seismic metamaterials: Low frequency rayleigh wave with extremely wide bandgaps. International Journal of Structural Stability and Dynamics 20 (14),
Oudich, M., Li, Y., Assouar, B.M., *et al.*, 2010. A sonic band gap based on the locally resonant phononic plates with stubs. New Journal of Physics 12 (8), 083049.
Oudich, M., Senesi, M., Assouar, M.B., *et al.*, 2011. Experimental evidence of locally resonant sonic band gap in two-dimensional phononic stubbed plates. Physical Review B 84 (16), 3–8.
Oudich, M., Djafari-Rouhani, B., Pennec, Y., *et al.*, 2014. Negative effective mass density of acoustic metamaterial plate decorated with low frequency resonant pillars. Journal of Applied Physics 116 (18), 184504.
Oudich, M., Djafari-Rouhani, B., Bonello, B., *et al.*, 2017. Phononic crystal made of multilayered ridges on a substrate for rayleigh waves manipulation. Crystals 7 (12), 372.
Oudich, M., Djafari-Rouhani, B., Bonello, B., *et al.*, 2018. Rayleigh waves in phononic crystal made of multilayered pillars: Confined modes, fano resonances, and acoustically induced transparency. Physical Review Applied 9 (3), 034013.
Pal, R.K., Ruzzene, M., 2017. Edge waves in plates with resonators: An elastic analogue of the quantum valley Hall effect. New Journal of Physics 19 (2), 025001.
Pendry, J.B., 2000. Negative refraction makes a perfect lens. Physical Review Letters 85 (18), 3966–3969.
Peng, B., Özdemir, Ş.K., Chen, W., *et al.*, 2014. What is and what is not electromagnetically induced transparency in whispering-gallery microcavities. Nature Communications 5 (1), 5082.
Pennec, Y., Djafari-Rouhani, B., Larabi, H., *et al.*, 2008. Low-frequency gaps in a phononic crystal constituted of cylindrical dots deposited on a thin homogeneous plate. Physical Review B 78 (10), 1–8.
Poddubny, A., Iorsh, I., Belov, P., *et al.*, 2013. Hyperbolic metamaterials. Nature Photonics 7 (12), 948–957.
Prosandeev, S., Lisenkov, S., Bellaiche, L., 2010. Kittel law in BiFeO(3) ultrathin films: A first-principles-based study. Physical Review Letters 105 (14), 147603.
Rayleigh, L., 1910. CXII. The problem of the whispering gallery. The London, Edinburgh, and Dublin Philosophical Magazine and Journal of Science 20 (120), 1001–1004.
Ren, X., Das, R., Tran, P., *et al.*, 2018. Auxetic metamaterials and structures: A review. Smart Materials and Structures 27 (2), 023001.
Rolland, Q., Oudich, M., El-Jallal, S., *et al.*, 2012. Acousto-optic couplings in two-dimensional phoxonic crystal cavities. Applied Physics Letters 101 (6), 061109.
Rupin, M., Lemoult, F., Lerosey, G., *et al.*, 2014. Experimental demonstration of ordered and disordered multiresonant metamaterials for lamb waves. Physical Review Letters 112 (23), 234301.
Rupin, M., Catheline, S., Roux, P., 2015. Super-resolution experiments on Lamb waves using a single emitter. Applied Physics Letters 106 (2), 024103.
Sigalas, M.M., Economou, E.N., 1994. Elastic-waves in plates with periodically placed inclusions. Journal of Applied Physics 75 (6), 2845–2850.
Sigmund, O., Jensen, J.S., 2003. Systematic design of phononic band-gap materials and structures by topology optimization. Philosophical Transactions A Mathematical, Physical and Engineering Sciences 361 (1806), 1001–1019.
Smith, D.R., Padilla, W.J., Vier, D.C., *et al.*, 2000. Composite medium with simultaneously negative permeability and permittivity. Physical Review Letters 84 (18), 4184–4187.
Su, X., Lu, Z., Norris, A.N., 2018. Elastic metasurfaces for splitting SV- and P-waves in elastic solids. Journal of Applied Physics 123 (9), 091701.
Tanaka, Y., Tamura, S., 1998. Surface acoustic waves in two-dimensional periodic elastic structures. Physical Review B 58 (12), 7958–7965.
Tang, K., Qiu, C., Ke, M., *et al.*, 2014. Anomalous refraction of airborne sound through ultrathin metasurfaces. Scientific Reports 4 (1), 6517.
Torrent, D., Mayou, D., Sánchez-Dehesa, J., 2013. Elastic analog of graphene: Dirac cones and edge states for flexural waves in thin plates. Physical Review B 87 (11), 115143.
Trzaskowska, A., Mielcarek, S., Sarkar, J., 2013. Band gap in hypersonic surface phononic lattice of nickel pillars. Journal of Applied Physics 114 (13), 134304.
Tsakmakidis, K.L., Boardman, A.D., Hess, O., 2007. 'Trapped rainbow' storage of light in metamaterials. Nature 450 (7168), 397–401.
Tsui, D.C., Stormer, H.L., Gossard, A.C., 1982. Two-dimensional magnetotransport in the extreme quantum limit. Physical Review Letters 48 (22), 1559–1562.
Vila, J., Pal, R.K., Ruzzene, M., 2017. Observation of topological valley modes in an elastic hexagonal lattice. Physical Review B 96 (13), 134307.
Wang, P., Lu, L., Bertoldi, K., 2015. Topological phononic crystals with one-way elastic edge waves. Physical Review Letters 115 (10), 104302.
Wang, T.-T., Wang, Y.-F., Wang, Y.-S., *et al.*, 2017. Tunable fluid-filled phononic metastrip. Applied Physics Letters 111 (4), 041906.
Wang, W., Jin, Y., Wang, W., *et al.*, 2020. Robust Fano resonance in a topological mechanical beam. Physical Review B 101 (2), 024101.
Williams, E.G., Roux, P., Rupin, M., *et al.*, 2015. Theory of multiresonant metamaterials forA0Lamb waves. Physical Review B 91 (10), 1–12.
Wu, T.T., Huang, Z.G., Tsai, T.C., *et al.*, 2008. Evidence of complete band gap and resonances in a plate with periodic stubbed surface. Applied Physics Letters 93 (11), 98–101.
Xiao, M., Ma, G.C., Yang, Z.Y., *et al.*, 2015. Geometric phase and band inversion in periodic acoustic systems. Nature Physics 11 (3), 240–244.
Xiao, Y., Wen, J., Wen, X., 2012. Flexural wave band gaps in locally resonant thin plates with periodically attached spring–mass resonators. Journal of Physics D Applied Physics 45, 19.
Yabin, J., Bernard, B., Yan, P., *et al.*, 2021. Physics of surface vibrational resonances: Pillared phononic crystals, metamaterials, and metasurfaces. Reports on Progress in Physics 84.
Yablonovitch, E., 1987. Inhibited spontaneous emission in solid-state physics and electronics. Physical Review Letters 58 (20), 2059–2062.
Yan, X., Zhu, R., Huang, G.L., *et al.*, 2013. Focusing Flexural Lamb Waves by Designing Elastic Metamaterials Bonded on a Plate. SPIE.
Yan, Z.Y., Wu, J.H., 2017. Ultra-low-frequency broadband of a new-type acoustic metamaterial beams with stiffness array. Journal of Physics D: Applied Physics 50 (35), 355104.
Yan, Z.Z., Wang, Y.S., 2006. Wavelet-based method for calculating elastic band gaps of two-dimensional phononic crystals. Physical Review B 74 (22), 224303.
Yang, Z., Gao, F., Shi, X., *et al.*, 2015. Topological acoustics. Physical Review Letters 114 (11), 114301.
Yu, X., Zhou, J., Liang, H., *et al.*, 2018. Mechanical metamaterials associated with stiffness, rigidity and compressibility: A brief review. Progress in Materials Science 94, 114–173.
Zaremanesh, M., Carpentier, L., Gharibi, H., *et al.*, 2021. Temperature biosensor based on triangular lattice phononic crystals. APL Materials 9 (6), 061114.
Zeighami, F., Palermo, A., Marzani, A., 2019. Inertial amplified resonators for tunable metasurfaces. Meccanica 54 (13), 2053–2065.
Zhang, X., Xiao, M., Cheng, Y., *et al.*, 2018. Topological sound. Communications Physics 1 (1), 97.
Zhang H-b, Chen J.-j, Han, X., 2012. Lamb wave band gaps in a homogenous plate with periodic tapered surface. Journal of Applied Physics 112 (5), 054503.
Zhao, H.J., Guo, H.W., Li, B.Y., *et al.*, 2015. Flexural vibration band gaps in a double-side phononic crystal plate. Journal of Applied Physics 118 (4), 044906.

Zhao, J., Bonello, B., Boyko, O., 2016. Focusing of the lowest-order antisymmetric Lamb mode behind a gradient-index acoustic metalens with local resonators. Physical Review B 93 (17), 174306.
Zhou, C., Sai, Y., Chen, J., 2016. Tunable Lamb wave band gaps in two-dimensional magnetoelastic phononic crystal slabs by an applied external magnetostatic field. Ultrasonics 71, 69–74.
Zhou, W., Wu, B., Muhammad, *et al*., 2018. Actively tunable transverse waves in soft membrane-type acoustic metamaterials. Journal of Applied Physics 123 (16), 165304.
Zhou, W., Su, Y., Muhammad, *et al*., 2020. Voltage-controlled quantum valley Hall effect in dielectric membrane-type acoustic metamaterials. International Journal of Mechanical Sciences 172.105368.
Zhu, J., Chen, Y., Zhu, X., *et al*., 2013. Acoustic rainbow trapping. Scientific Reports 3 (1), 1728.
Zou, K., Ma, T.-X., Wang, Y.-S., 2016. Investigation of complete bandgaps in a piezoelectric slab covered with periodically structured coatings. Ultrasonics 65, 268–276.